

An overview on the Urban Boundary-layer Atmosphere

Network in Helsinki

Wood CR^{1*}, Järvi L², Kouznetsov RD^{1,4}, Nordbo A², Joffre S¹, Drebs A¹, Vihma T¹, Hirsikko A^{1,#},
Suomi I¹, Fortelius C¹, O'Connor E^{1,3}, Moiseev D^{1,2}, Haapanala S², Moilanen J², Kangas M¹, Karppinen
A¹, Vesala T², Kukkonen J¹

¹ Finnish Meteorological Institute, Erik Palménin aukio 1, FI-00101, Helsinki, Finland

² Department of Physics, University of Helsinki, FI-00014, Helsinki, Finland

³ Department of Meteorology, University of Reading, RG6 6BB, Reading, United Kingdom

⁴ Obukhov Institute of Atmospheric Physics, Pyzhevski per. 3 119017 Moscow, Russia

Currently at: Forschungszentrum Jülich GmbH, Institut für Energie-und Klimaforschung:
Troposphäre (IEK-8), Jülich, Germany.

* curtis.wood@fmi.fi, +358 504058034

Keywords – urban meteorology, urban climate, boundary layer, surface turbulent fluxes, lidar,
sodar, scintillometer, sonic anemometer, eddy covariance, ceilometer

1 **Abstract**

2 Helsinki UrBAN (Urban Boundary-layer Atmosphere Network, <http://urban.fmi.fi>) is a dedicated
3 research-grade observational network where we study the physical processes in the atmosphere above
4 the city. Helsinki UrBAN is the most poleward intensive urban research observation network in the
5 world and thus will allow studying some unique features such as strong seasonality. The network's key
6 purpose is for the understanding of the physical processes in the urban boundary layer, and associated
7 fluxes of heat, momentum, moisture, and other gases. A further purpose is to secure a research-grade
8 database, which can be used internationally to validate and develop numerical models of air quality and
9 weather prediction. We use scintillometers, a scanning Doppler lidar, ceilometers, a sodar, eddy-
10 covariance stations, and radiometers. This equipment is supplemented by auxiliary measurements,
11 which were primarily set up for general weather and/or air-quality mandatory purposes, such as vertical
12 soundings and the operational Doppler radar network. Examples are presented as a testimony to the
13 potential of the network for urban studies, such as (i) evidence of a stable boundary layer possibly
14 coupled to an urban surface, (ii) the comparison of scintillometer data with sonic anemometry above an
15 urban surface, (iii) the application of scanning lidar over a city, and (iv) combination of sodar and lidar
16 to give a fuller range of sampling heights for boundary-layer profiling.

17 **Capsule**

18 Helsinki UrBAN (Urban Boundary-layer Atmosphere Network, <http://urban.fmi.fi>) is a dedicated
19 intensive research-grade observational network for the study of the physical processes in the
20 atmosphere above high-latitude Helsinki, Finland.

21 **Front Page Background Photograph**

22 We uploaded a photograph as a candidate for the background of the first page of the article.

23

1 Although urban areas comprise a very small fraction of Earth's land cover (Schneider et al. 2009), over
2 half of global population live in urban agglomerations. Therefore, it is important to monitor,
3 understand, and predict the modifications occurring in local weather and climate due to urbanization—
4 particularly for the perspective of accurate high-resolution weather and air-quality forecasting and
5 climate-sensitive urban design and planning. Cities are characterized by a high fraction of impervious
6 surfaces, which modify both surface energy and water balances—further affecting atmospheric-
7 boundary-layer (ABL) turbulence and weather processes. Cities are also the main *area sources* of air
8 pollutants with detrimental effects on human health and comfort. Cities can generate, modify, and/or
9 amplify many processes behind global changes such as increases in greenhouse-gas concentrations,
10 increased water and energy demand, environmental pollution, or change of biodiversity. Moreover, the
11 recent increase of spatial resolution in numerical weather prediction (NWP) models and the improved
12 treatments of model physics and chemistry in NWP and chemical-transport models, demands a more
13 realistic representation of urban features, processes, and feedbacks in these models (Kukkonen et al.
14 2012). Therefore, we need dedicated and long-term monitoring of urban meteorological processes.

15 Long-term urban ABL observations at different spatial and temporal scales using various instruments
16 have been made in few cities (Rotach et al. 2002; Grimmond 2006), and most studies have not used
17 state-of-the-art equipment for long periods. Since the pioneering METROMEX urban study in St
18 Louis (Changnon et al. 1971), the more recent comprehensive studies include the cities of Basel in
19 Switzerland (Rotach et al. 2005), Marseille in France (Cros et al. 2004), Oklahoma City in USA (Allwine
20 and Flaherty 2006), New York in USA (Hanna et al. 2006), Toulouse in France (Masson et al. 2008),
21 Montreal and Vancouver in Canada (<http://www.epicc.ca>), and London in UK (Wood et al. 2009;
22 Harrison et al. 2011). Most studies have focused on specific campaigns, often with less than one year of
23 measurements—and have concentrated on mid-latitude cities. To date, most high-latitude urban ABL
24 research has used solitary, or few, point measurements (Eresmaa et al. 2006; Mårtensson et al. 2006;
25 Lemonsu et al. 2008; Vesala et al. 2008; Järvi et al. 2009a; Bergeron and Strachan 2012; Nordbo et al.
26 2012a). Thus, there is a clear lack of intensive research-grade long-term ABL observations, especially

1 from high-latitude cities—with their associated pronounced annual variations in meteorological
2 conditions and continuous snow-cover that can last several months (Lemonsu et al. 2010). These
3 conditions might create extreme meteorological conditions such as e.g. strong ground-based or elevated
4 inversions (Kukkonen et al. 2005) with detrimental air-quality implications.

5 An extensive mesoscale effort (Helsinki Testbed) centered around the Helsinki Metropolitan Area has
6 been running several years (core data years 2005–2009) covering 150 x 150 km² area of southern
7 Finland and northern Estonia (Koskinen et al. 2011). In addition to this mesoscale observational
8 network, the urban measurement station SMEAR-III has been running in Helsinki since 2004 (Järvi et
9 al. 2009b). The station concentrates on observing surface–atmosphere exchange processes at a
10 micrometeorological scale, in particular using the eddy-covariance (EC) method to directly measure
11 vertical turbulent fluxes of momentum, sensible, and latent heat, and carbon dioxide (Vesala et al. 2008;
12 Järvi et al. 2012; Nordbo et al. 2012a,b).

13 Combining those observations with additional state-of-the-art observations has enabled a new
14 observational research-intensive network: Helsinki UrBAN (Urban Boundary-layer Atmosphere
15 Network, <http://urban.fmi.fi>). Our aim is that the network will improve our understanding of urban
16 ABLs by including measurements of a wide variety of processes at a range of scales. The observations
17 in the network are complemented with model developments, such as NWP and urban-energy-balance
18 modeling (see online supplemental material).

19
20 The long-term purposes of Helsinki UrBAN are to:

- 21 1. Understand the processes in Helsinki's ABL, as affected by a range of surfaces within a few
22 kilometers (urban, suburban, and sea) and the strong climatic seasonality.
- 23 2. Provide better experimental data for developing and evaluating numerical models such as NWP,
24 meteorological pre-processing, and air-quality models (see online supplemental material).

1 3. Provide results that will support improvements in relevant applications such as city planning,
2 building design, and energy use.

3 The aim of this article is to describe the network, show selected results, and remark on potential future
4 use of the results of the network.

5 **THE NETWORK**

6 An overview of observing site locations and instrumentation for studying Helsinki's ABL is displayed in
7 FIG. 1 and TABLE 1. We define downtown Helsinki as the central area of buildings that are densely-
8 packed with a regular layout (Nordbo et al. 2012a), i.e. approximately the land area south of 60.18°N
9 (encompassing the observation sites of Tornio, Fire Station, Sitra, and Kaisaniemi).

“SideBar”: CLIMATE AND TOPOGRAPHY OF HELSINKI

Helsinki, the capital city of Finland, had approximately 596000 inhabitants in 2012 (density 2789 km⁻²), although the Helsinki Metropolitan Area (defined as the municipalities of Helsinki, Espoo, Vantaa, and Kauniainen) has about 1.1 million inhabitants (1377 km⁻²) (Population Register Center of Finland 2012). Helsinki is located on the north shore of the Gulf of Finland in the Baltic Sea. Due to the influence of the vicinity of the sea—and oceanic-scale features such as the North Atlantic Drift—winter temperatures are higher than the far northern location might suggest, resulting in a humid continental climate (Köppen–Geiger climate classification Dfb). The annual mean air temperature is +5.9 °C (period 1981–2010), with the lowest monthly average temperature in February of –4.7 °C and the highest monthly average temperature in July of +17.8 °C (Pirinen et al. 2012). Monthly average sunshine hours vary from 25 hours in December to 280 hours in June. Precipitation amounts are moderate, the average annual precipitation sum is 655 mm: with the highest monthly average in August (80 mm), the lowest in April (32 mm). The average number of days with precipitation exceeding 1 mm varies all year round from 7 to 12 days per month. Due to the vicinity of the Gulf of Finland, long spells of dry and hot weather are rare—unless synoptic conditions dictate such as, for example, a long period of easterly flow occurs in the summer.

In winter, the sea is typically ice-covered, but can be open or partly open. In winter conditions of an open sea during cold-air outbreaks, the sea surface may be 20–30°C warmer than the air above it. This may result in turbulent fluxes of sensible and latent heat totaling several hundreds of W m⁻², resulting in a development of a convective boundary layer (Vihma and Brümmer 2002; Tammelin et al. 2012). In summer, the sea surface temperature may vary in time and space due to upwelling in the sea. During coastal upwelling, the sea surface temperature may rapidly drop by up to 10°C, causing stabilization of the ABL and fog formation (Suomi 2004).

Topographical changes in Helsinki are very slight and most of the metropolitan area is less than 50 m above mean sea level (a.s.l.). Helsinki has heterogeneity at the kilometer scale with urban, suburban, forest, grassland, sea (open or frozen) (FIG. 1). Most of the city is low-rise: with few buildings above 60 m.

1 *In-situ equipment and main sites*

2 The eddy-covariance (EC) measurements of turbulent fluxes are made at three sites in Helsinki:
3 Kumpula, Fire Station, and Tornö.

4 On the Kumpula campus, next to the Finnish Meteorological Institute (FMI) and University of
5 Helsinki buildings, is the SMEAR-III mast (*Station for Measuring Ecosystem-Atmosphere Relations*, Järvi *et al.*,
6 2009b). This semi-urban site, located around 4 km north-east from downtown Helsinki, has developed
7 as a core site of focused activity for inter-comparison of instruments and a deeper understanding of
8 processes at one site. EC measurements at Kumpula have been on-going since 1st December 2005
9 (Vesala *et al.* 2008; Järvi *et al.* 2009b,c). The flux measurements are carried out atop a 31-meter-high
10 lattice mast (the base being 26 m a.s.l.), with possible mast flow distortion from 0–50°. It is
11 characterized as a semi-urban measurement site, given that three different surface cover areas (road,
12 vegetation, built) can be distinguished within about a kilometer around the mast, allowing separate
13 analysis of fluxes for those upwind surfaces. The mean height of the nearby buildings (z_H) in the built
14 sector is 20 meters (and only 8.4 m averaged for the whole sector within 1 km radius), so the flux
15 measurements are carried out at $1.6z_H$ with respect to the nearby buildings. Detailed description of the
16 site and measurements can be found elsewhere (Vesala *et al.* 2008; Järvi *et al.* 2009c; Nordbo *et al.*
17 2012a).

18 The other two EC sites, Fire Station and Tornö, are located downtown within a distance of only 500
19 meters from each other (Nordbo *et al.* 2012a). Those locations are among the highest possible locations
20 in downtown Helsinki; and their source areas can be estimated at about a kilometer radius depending
21 on atmospheric stability and wind direction (Nordbo *et al.* 2012a). At the Fire Station, flux
22 measurements began on 28th June 2010 (the measurements had to stop on 27th January 2011 due to
23 building refurbishments, and to date have not resumed yet). Measurements were made on top of the
24 38-meter-high tower (the base is 23 m a.s.l.) with mast flow distortion from 90–180°. The tower itself is
25 8.8 m x 8.8 m, and a pole was installed on top of it in north-west corner so that the measurements were

1 carried out 42 meters a.g.l. (above ground level). At Tornio, the measurements have been on-going since
2 28th September 2010. The measurements are made 60 m a.g.l. (ground at 15 m a.s.l.) with mast flow
3 distortion from 50–185°, where a 2.3 meter high pole is installed. The details of these measurements –
4 including building configuration, instrumental layout, and footprint analysis – can be found in Nordbo
5 et al. (2012a). The surrounding area of both sites is highly built-up with the fraction of impervious
6 surfaces, including buildings and paved surfaces, being above 80% inside a 1-km-radius circle. In
7 downtown Helsinki, buildings are reasonably well-packed and uniform and variation as a function of
8 wind direction within the footprint of Tornio EC site are: mean building heights $z_{H1} = 19\text{--}29$ m,
9 aerodynamic roughness length $z_0 = 0.9\text{--}1.9$ m, and zero-plane displacement height $z_{d1} = 12\text{--}18$ m
10 (following morphological methods from building databases; Nordbo et al. 2012a). The building height
11 and roughness length do not vary much with distance from the tower (thus reducing uncertainty in
12 source-area estimates), although they vary slightly as a function of wind direction. Both downtown EC
13 stations are at about 2–3 times the mean building height, and $9\text{--}50 (z - z_{d1})/z_0$ (Nordbo et al. 2012a). For
14 comparison, although there are EC measurements at a range of heights within and above the urban
15 canopy across the globe, most urban EC sites range between $0.4\text{--}500 (z - z_{d1})/z_0$ and up to $22z_{H1}$ (Roth
16 2000; Nordbo et al. 2012a).

17 At all three EC sites, the fluxes (of momentum, sensible heat, latent heat, CO₂ and aerosol particle
18 number) are measured with the well-established EC method (Aubinet et al. 2012). The configurations
19 comprise a three-dimensional sonic anemometer, infrared gas analyzers for measuring the CO₂ and
20 water-vapor fluctuations, and water condensation particle counters for measuring particle number
21 concentrations. Raw eddy-covariance data are logged at 10 Hz for post processing, and fluxes are
22 calculated with 30-minute averaging according to standard methods (Nordbo et al. 2012c).

23 Furthermore, values of the structure parameter of temperature (C_{Tz}) are estimated from 10-Hz time
24 series of instantaneous sonic temperature measured by the sonic anemometers. Data from sonic
25 anemometers and scintillometers (see below) can thence be readily compared using C_{Tz} . The spectrum-

1 model-fitting method (Kouznetsov and Kallistratova 2010; Wood et al. 2013a) is used with 1024-point
2 (10 s) segments over 10-minute intervals. The method uses the Welch-periodogram spectra to fit the
3 model spectrum that accounts for the internal noise of measurements and for the Nyquist effect of
4 sampling. The approach implicitly assumes stationarity of the sonic data series.

5 Comprehensive aerosol particle and gas pollutant measurements are carried out at Kumpula. These
6 include size-resolved aerosol particle number concentration, ozone, nitrogen oxides, carbon monoxide,
7 and sulfur dioxide (Hussein et al. 2008; Järvi et al. 2009b), as well as detailed aerosol chemical
8 composition (Saarnio et al. 2010). Turbulent fluxes of total number concentration are measured both at
9 Kumpula (Järvi et al. 2009d; Ripamonti et al. 2013) and Tornio. A summary of the range of air-quality
10 observations across the Helsinki Metropolitan Area (HSY) can be found elsewhere (www.airquality.fi).
11 Briefly, air quality is monitored at eleven stations (seven permanent, four mobile), with live HSY
12 website updates. Typical observations include PM_{10} , $PM_{2.5}$, nitrogen dioxide, nitrogen monoxide, ozone,
13 sulfur dioxide, volatile organic compounds, and carbon monoxide.

14 Additional measurements made at Kumpula include wind and temperature profiles at heights 4, 8, 16,
15 and 32 meters. Other measurements include the radiation components and photosynthetically-active
16 radiation, at 31 meters height.

17 Downtown, on a lattice mast 90 m east of the Fire Station tower (FIG. 1), a radiation-balance sensor
18 and two radiation thermometers are mounted at 53 meters a.g.l. and about 30–40 meters above roof
19 level of surroundings. The primary purpose of the radiation thermometers is to provide a reference for
20 the thermal camera readings (see below) and to evaluate the effect of spatial inhomogeneity on integral
21 thermal properties of the urban surface. One of the radiation thermometers is looking westward at the
22 camera's field of view and another one 45 degrees below the camera-view axis.

23 In addition, four infrared radiation sensors have been mounted at Tornio to measure surface
24 temperatures of four surfaces in different orientations. They are located at 36–38 meters a.g.l. They are
25 measuring a black sheet-metal roof, a concrete floor, and concrete walls.

1 Finally, FMI has several operational automatic weather stations across Finland that record temperature,
2 humidity, wind speed and gusts, precipitation, cloud coverage, wind direction, atmospheric pressure,
3 snow depth, and visibility. Around 10 of these are within the area on FIG. 1a. Two reference sites
4 worthy of mention include Kaisaniemi – where air temperature has been recorded since 1838 – and
5 Helsinki-Vantaa airport, useful for inland conditions (FIG. 1).

6 *Spatially-resolving and Spatially-averaging Equipment*

7 A single-antenna vertical sodar (Kouznetsov 2007, 2009) was located at Kumpula (on the FMI roof)
8 from 14th August 2009 to 5th September 2011, but was moved westward 2.3 km to another semi-urban
9 site (Pasila) from 29th March 2012 onwards. The repetition frequency is 5 seconds, and the sounding
10 range is 20–400 m above the antenna, with a vertical resolution of 10 m. The Doppler shift of the
11 echo-signal is used to evaluate the vertical-velocity component. During the echo-signal processing for
12 each range-gate, the scattering intensity and the velocity are evaluated. To distinguish the echo-signal
13 from the noise, the noise level is evaluated in adjacent frequency bands. The two key outputs are (i)
14 profiles of vertical velocity variance, and (ii) the diagnosis of ABL depth when it is within the sodar's
15 range using the minimum in backscatter gradient profile (Wood et al. 2012).

16 A pulsed scanning Doppler lidar (Pearson et al. 2009) has been operating at Kumpula (on FMI roof)
17 since 1st September 2011 operating at 1.5- μ m wavelength and equipped with a depolarization channel
18 receiving backscattering signal from aerosol particles and hydrometeors, i.e. cloud/fog droplets and ice
19 crystals. Primary data processing includes noise removal from clear sky data based on signal-to-noise
20 ratio and a standard self-calibration procedure (O'Connor et al. 2004). The observation range is 90–
21 9600 m, with 30 m resolution. Low aerosol concentration—typical for poleward sites—affects lidar
22 data quality, which requires careful optimization of integration time and beam focus. Data availability is
23 variable, but since typically a 5-second interval or longer time is needed to improve the signal-to-noise
24 ratio; the current integration time is 20 seconds. In addition to vertical profiles of aerosol and vertical
25 velocity, Doppler scanning (beam swinging) techniques enable the collection of vertical profiles of

1 horizontal wind speed vectors. Novel scanning strategies may enable the study of estimates of a
2 horizontal transect of horizontal wind vectors (Wood et al. 2013b), turbulent mixing and dynamics of
3 the ABL (Barlow et al. 2011), and sensible heat and momentum flux (Collier et al. 2005). Performance
4 of the lidar was investigated during a two-week inter-comparison campaign in Helsinki (Hirsikko et al.
5 2013) against FMI's other Doppler lidars showing good agreement for the wind vector profiles. From
6 2013 onwards, these ABL wind and aerosol profiles will be complemented with a sodar-RASS
7 instrument for temperature and wind profiles.

8 FMI has five operational ceilometers within 50 km of central Helsinki: Kumpula, Helsinki-Vantaa
9 airport (ca. 14 km north), Isosaari island (ca. 8 km south-east, ca. 7 km off the Finnish coast),
10 Nurmijärvi (ca. 50 km north of downtown Helsinki), and Porvoo (ca. 50 km east) but are configured to
11 provide just cloud base. Two ceilometers have continuously logged profile measurements: at Kumpula
12 from 22nd June 2009 onwards (Vaisala CL31), and at the FMI radiosounding observatory of Jokioinen
13 (about 100 km north-west of Helsinki, Vaisala CL51). In addition, some theoretical investigations have
14 been performed using ceilometer profile data from specific experiments in suburban Helsinki (Vaisala,
15 Vantaa, FIG. 1) to estimate ABL depth (Eresmaa et al. 2006, 2012).

16 Two Boundary Layer Scintillometers (BLS900) were installed in central Helsinki. A 4.1 km 'city-scale'
17 path has been operating since 5th July 2011 on a near south–north path from downtown (Torni) to
18 semi-urban Kumpula (198° bearing) and the beam is about 40–60 meters a.g.l. (ca. 10–40 m above
19 building height). The second 'downtown' BLS was installed on 2nd March 2012 in a roughly east-west
20 1.8 km path across downtown Helsinki at a height of 50–70 meters a.g.l. (271° bearing) from the Fire
21 Station mast to the Sitra building. The Sitra building is located on the western edge of the densely-
22 packed buildings downtown. The source area of the second scintillometer is downtown and thus
23 qualitatively corresponds to much of the source area of the downtown (Torni) EC measurements,
24 where building heights are 19–29 m. These scintillometers give a spatially-integrated value of the
25 refractive-index structure parameter (C_{n^2}) and cross-beam horizontal wind component. C_{n^2} can readily

1 be converted to C_{T3} , but conversion to sensible heat flux requires many assumptions and is most-readily
2 applied only during free convection (Zeweldi et al. 2009). The path-weighting of the instrument is such
3 that most of the signal comes from the center of the beam (Hill and Ochs 1978; Kipp and Zonen
4 2005). The scintillometer measurements require good visibility, thus no data comes during fog or
5 precipitation (Uijlenhoet et al. 2011).

6 An infra-red camera is installed on the Fire Station mast with a westward view across downtown in
7 order to cover a part of the footprint of the Tornø EC and the downtown scintillometer measurements.
8 The camera has 48x47 pixels and 60x60 degree view area. This results in effective horizontal resolution
9 of about 10 meters close to the camera. The images are acquired and stored every 5 seconds. No
10 corrections are yet applied to the camera data. Despite the absolute thermal accuracy being poor (± 3
11 K), thermal inhomogeneities within a fraction of a degree can be measured. The camera is affected by
12 the thermal anisotropy of the urban surface and thus should be used with care. Therefore, it is more
13 useful for relative comparison of thermal sources in any investigated direction in order to help for the
14 analyses of scintillometer data, or case studies.

15 These spatially-averaging instruments are a key addition to point measurements in order to assess
16 model grid values. Helsinki UrBAN will support FMI's goal of developing within the HIRLAM-
17 ALADIN framework its new operational non-hydrostatic HARMONIE limited area model with 2.5
18 km horizontal resolution that includes the urban Town Energy Balance module (Masson 2000).
19 Supporting information on model developments along with more details on instrument manufacturers
20 and a summary of some auxiliary instruments to Helsinki UrBAN are provided in the online
21 supplemental material.

22 **OBSERVATIONS OF HELSINKI'S ATMOSPHERE**

23 We now present examples as a testimony to the potential of the network.

1 *Seasonality and diurnal cycle*

2 One of the main drivers determining the climate of Helsinki is the strong seasonality of net all-wave
3 radiation (Q^*). A greater daytime Q^* is observed downtown than at semi-urban Kumpula for most
4 times in the year and day (FIG. 2a). In late winter (Jan–Mar), the lower Q^* values are mainly caused by
5 the snow cover which increases the surface albedo and causes a large amount of $K\uparrow$ (FIG. 2b), especially
6 at the semi-urban Kumpula site; whereas less snow is observed downtown. We hypothesize that the
7 large difference is due to: (i) the extensive snow clearing from roads, footpaths, and roofs downtown;
8 and (ii) energy balance differences such as increased long wave radiation from the vertical snow-free
9 walls, building heat storage, and anthropogenic heat emissions. During snow free periods (May–
10 October), the surface albedo is slightly higher at Kumpula (0.13 ± 0.01) compared to downtown (0.11
11 ± 0.01). This higher albedo can be explained by the higher fraction of vegetation cover in Kumpula as
12 vegetation has typically higher reflectivity than built surfaces (Oke 1987). Interestingly, only slightly
13 higher upward longwave radiation is measured downtown than Kumpula (not shown). Lower Q^* in
14 Kumpula could also be explained by atmospheric pollutants or humidity, which might affect the
15 downward radiation components especially in spring when typically intensive re-suspension of road
16 gravel takes place (Kupiainen et al. 2011). However, since Helsinki's air pollution is typically relatively
17 low (except in spring; Järvi et al. 2009b), this would require more-detailed investigations with respect to,
18 e.g., wind direction, thus yielding possible explanations from the prevailing downwind position of
19 Kumpula with regards to downtown during these months and/or from local sources of pollution,
20 moisture, or secondary organic particles (from vegetation). The large wintertime difference in $K\uparrow$
21 between downtown and Kumpula emphasizes the importance of snow in the radiation balance and
22 further in the energy partitioning and in energy balance models. Previously, this has been only
23 marginally studied (Lemonsu et al. 2008, 2010; Bergeron and Strachan 2010) and thus our network
24 could provide important data for developing and assessing snow processes' parameterization in
25 atmospheric models.

1 The pattern of net all-wave radiation translates into the sensible heat flux (Q_H), which also experiences
2 strong annual and diurnal variation (FIG. 3). First, it is perhaps obvious that the greatest sensible heat
3 fluxes, of above 150 W m^{-2} at both sites, are observed in May–August during the daytime hours of
4 06:00–14:00 (all times are in hours UTC). At Kumpula, there is little annual variation of sensible heat
5 flux by night: the average is negative, although the average nocturnal sensible heat flux in winter is near
6 zero. Downtown, the winter nights exhibit a mean positive sensible heat flux, although some cases of
7 negative sensible heat flux can occur (see later case study). The strongest diurnal cycles in sensible heat
8 flux occurred in spring and summer (especially downtown). In winter, there is very little diurnal
9 variation in the mean sensible heat flux at both sites especially under the cloudy snow-free conditions
10 of November–December 2011. This is consistent with the near-zero net all-wave radiation (FIG. 2).
11 When comparing the two sites, we see how the difference in sensible heat fluxes has a patchy pattern:
12 the largest values occurring in late April – early May, between 08:00 and 12:00, with fluxes at Kumpula
13 higher by over 50 W m^{-2} than downtown (also in 2012, not shown). At the same time, very high latent
14 heat fluxes were not observed downtown, so we hypothesize these low Q_H values downtown could be
15 caused by heat storage flux to the cold building walls in spring. The storage heat flux typically peaks
16 before mid-day and thus reduces available energy consumed in Q_H (Grimmond et al. 1991). This can be
17 verified in future when the seasonal behavior of the storage heat flux will be examined by modeling
18 approaches. A diurnal pattern is also seen when comparing the two sites: greater daytime sensible heat
19 fluxes are observed downtown than for Kumpula; this is likely a result of several factors including
20 higher Q^* , anthropogenic heat emissions and heat storage, advection from the sea, and energy
21 partitioning caused by a high fraction of vegetation at Kumpula.

22 *A clear diurnal-cycle case study: 4th September 2011*

23 To observe the evolution of the Helsinki ABL characteristics during a diurnal cycle, a day is chosen in
24 the autumn with high atmospheric pressure (maximum 1015 hPa) and fair-weather cumulus (FIG. 4). A
25 clear diurnal cycle is observed in many variables, such as relative humidity and upwelling longwave

1 radiation—notwithstanding some additional synoptic changes: increase in wind speed and veer of wind
2 with time.

3 Patterns in the thermal IR camera data clearly show the main features of a warm surface by day and
4 cool by night (FIG. 5). But there is variability across the urban surface, primarily since surfaces facing
5 different directions receive different solar irradiance. By day, a sharp temperature difference can be
6 seen between the urban surface and the atmosphere, and a gradient in the atmosphere can also be seen
7 which is consistent with nearby vertical profiles of temperature (FIG. S1). The nocturnal IR data show
8 a much more even distribution of temperature across the urban surfaces, compared with the values
9 from the daytime. One possible implication is that modeling of daytime ABL conditions will require
10 either high horizontal resolution or suitable aggregation of inhomogeneous forcing from the surface;
11 while at night, vertical resolution would be more important. The IR camera could also be used to study
12 the urban-specific anthropogenic snowmelt from roofs that we hypothesize from FIG. 2b.

13 The evolution of ABL depth follows the expected pattern for clear-sky conditions (FIG. 6). A shallower
14 ABL is observed with the sodar for stable/night-time conditions between 100 and 150 m
15 (unobservable by the lidar due to blind region 0–120m). By day, the ABL grows to a depth of greater
16 than 400 m and is thus not observable with the sodar, the vertical profile of velocity variance in the
17 lidar data indicate that the ABL depth was probably over 1 km (crude estimation based on vertical
18 velocity variance limit of $0.1 \text{ m}^2 \text{ s}^{-2}$, Barlow et al. 2011). There is temporal agreement in the turbulence
19 regimes in the lidar and sodar: turbulence maximum by day and quiescent by night. However, due to
20 signal-to-noise constraints in the sodar velocity estimates, a quantitative comparison of vertical velocity
21 cannot be made on this occasion. It is a major strength of an integrated observation network that we
22 are able to observe the majority of shallow and deep ABLs by using both sodar and lidar at the same
23 site, but also to quantify on a long-term basis their differentiated observation methods of atmospheric
24 vertical structure inhomogeneities as a function of synoptic, stability, and surface conditions.

25 Nevertheless, on some occasions the ABL depth cannot be determined since it is below even the height

1 range of the sodar. Thus, a new lidar scanning technique within Helsinki UrBAN to cover these events
2 is under development, since shallow ABLs are especially important for urban air quality.

3 The diurnal evolution is clearly seen in the time series of structure parameter of temperature (FIG. 7b).
4 The greatest values (above $10^{-2} \text{ K}^2 \text{ m}^{-2/3}$) are seen in the daytime, and the greatest values occur
5 downtown as we would expect on the basis of greater positive sensible heat fluxes (FIG. 7a). On the
6 other hand, the scintillometer curve does not follow the average C_{T^2} values retrieved from downtown
7 (Torni) and Kumpula sonics (at both ends of the scintillometer path), except late morning. We
8 hypothesize that there is always some temperature gradient along the longer scintillometer beam due to
9 the difference in stability cycle between downtown and semi-urban sites. This motivates detailed
10 interpretation of the scintillometer path-weighting together with footprint analysis, and for additional
11 point measurements between Kumpula and downtown.

12 The day-time unstable stratification lasts several hours longer downtown, particularly due to a later
13 evening transition. The Kumpula time series of Q_H goes from unstable through neutral (with $C_{T^2} < 10^{-4}$
14 $\text{K}^2 \text{ m}^{-2/3}$) to stable (with $C_{T^2} \approx 10^{-3} \text{ K}^2 \text{ m}^{-2/3}$ after 19:00), while downtown (Torni) the heat flux and C_{T^2}
15 show a longer period of neutral conditions. Persistence of neutral conditions may have been caused by
16 greater anthropogenic heat release downtown and/or the evening increase in wind velocity observed
17 downtown, but not at Kumpula (FIG. 4b). The diurnal maximum in anthropogenic heat is usually
18 observed after working hours, which coincides with the persistent positive Q_H downtown between
19 15:00–18:00 (Sailor 2011).

20 It is noteworthy that sensible heat flux values are slightly positive or zero from 00:00–06:00, while at
21 16:00–24:00 they go negative (stratification increasing) at both downtown and Kumpula sites. On the
22 other hand, C_{T^2} values are closer together in the morning but strongly differ in the evening with the
23 downtown values plummeting before settling. The semi-urban (Kumpula) C_{T^2} curve resets to its level as
24 per morning (consistent with the same ABL depth estimates in morning and evening from sodar), while
25 downtown the low C_{T^2} value might indicate a different ABL height. These data show the interest of

1 combining the different measuring approaches, which can reveal subtle differences even within a few
2 kilometers range.

3 There are also possible complexities introduced by mesoscale changes such as topographical
4 differences, varying closeness of sea bays along the path. Most scintillometer work has been conducted
5 over homogeneous terrain (Moene et al. 2009). These preliminary results of structure parameters
6 determined from different techniques over heterogeneous terrain indicate an overall qualitative
7 agreement (Wood et al. 2013a); but on the other hand, subtle differences open opportunities for more
8 detailed investigations and understanding of intra-urban processes

9 Given the evolution of C_{T^2} and Q_{H^2} , it is interesting that stable boundary layers might be coupled to a
10 highly urbanized surface (<10% occurrence downtown of negative Q_{H^2}). Even downtown (Torni) has
11 occasionally stable flow (Nordbo et al. 2012a), perhaps partly explained by a small anthropogenic heat
12 flux, more sustainable use of energy, and climatology.

13 *A stable-atmosphere case study: 3rd January 2012*

14 Given the interest in stably-stratified flow above a city, a second case study was chosen specifically
15 where the Kumpula station had negative sensible heat fluxes even during daylight hours while the
16 downtown station (Torni) had negative fluxes at night and for a short period in the afternoon (FIG. 8a).
17 Despite the negative Q_{H^2} , the buoyancy term is very small in the turbulent kinetic energy budget (FIG.
18 8c) and it does not destroy the mechanically generated turbulence that is balanced out mainly by
19 dissipation. The large mechanical production is urban-specific, since the rough surface induces a high
20 momentum flux. As a result, atmospheric stability is suppressed toward neutral in comparison with a
21 less-rough surface with an equivalent sensible heat flux. Some of the changes in stability are consistent
22 with changes in cloud cover (FIG. 9), such as the stability going more stable between 04:00–07:00 when
23 the sky was clear (Illingworth et al. 2007). There are few reports of stable stratification over cities
24 (Fisher et al. 2005; Wood et al. 2010; Bergeron and Strachan 2012)—our observations of stable

1 stratification (13% in 2011 at Torni, FIG. 3) motivate further our network due to a link to air quality:
2 the largest particle fluxes and concentrations are observed at times of stability transition from stable to
3 neutral (FIG. 8d,e). Nevertheless, it is hard to distinguish the effect of atmospheric stability versus that
4 of traffic release since the stability transition and rush-hour take place around the same time. Analyzing
5 together atmospheric stability with traffic data will lead to an improved ability to predict Helsinki's air
6 quality. One of the main purposes of the network is to improve the description of urban surface and
7 the ABL in air-quality models, since stable urban ABLs are rarely observed in cities.

8 The lidar's custom scanning strategy allows a comparison between lidar and mast winds (Kumpula and
9 downtown). The lidar operated a 10-second sample every 5 minutes pointing due south at zero
10 elevation. The data from the first usable range-gate (#4) was compared with the northward component
11 of horizontal wind from Kumpula (FIG. 10). Reassuringly a small rmse of 0.5 m s^{-1} (with respect to 0–8
12 m s^{-1} v-component winds on this day) was observed for the 30-min mean values on this day—indeed
13 we would even expect some difference given the different spatial and temporal sampling of the two
14 instruments. This highlights the potential of ground-based scanning lidar to reveal flow features over a
15 city.

16 SUMMARY

17 The importance of long-term research-grade observations of the urban ABL has led to the
18 development of Helsinki UrBAN (<http://urban.fmi.fi>). This observation network has begun to
19 improve our understanding of Helsinki's ABL. Components of the network have been running since
20 2004, with substantial expansion in 2010–2012. New equipment has been installed during the last few
21 years: EC stations, scintillometers, sodar, lidar, and thermal IR camera.

22 Naturally, the network also has inherent limitations. (i) Although there are numerous non-urban
23 background reference sites, these either have not been equipped with the same instrumentation as the
24 corresponding urban sites (e.g., the radio tower measurements at the site of Kivenlahti, about 10 km
25 west of downtown Helsinki; see online supplemental material), or are located at a substantial distance

1 (such as SMEAR-II station at Hyytiälä, southern Finland, about 200 km north; Suni et al. 2003). (ii) The
2 coastal location of Helsinki complicates the distinction of urban effects (Lowry 1977). However, 38%
3 of global population live within 50 km of the coastline (Kay and Alder 2005), increasingly many of
4 them in urban environments. So although the meteorology of coastal regions is more challenging to
5 study than that of homogeneous inland sites, there is an evident need to study them (Mestayer et al.
6 2005). (iii) There are currently no in-canopy-layer measurements that would allow linking ABL climates
7 to the canopy layer. Helsinki was selected as the location of this network mainly since it forms the
8 largest urban agglomeration in Finland (the Helsinki Metropolitan Area), and also due to logistical
9 reasons (the location of the headquarters of the FMI and the University of Helsinki).

10 Data were shown to represent the potential of intensive state-of-the-art observations of the urban ABL.
11 The results showed the range of stabilities for diurnal and annual cycles both downtown and at a semi-
12 urban site: in particular, the seasonal cycle is pronounced. These results also show clear differences
13 between sites at even modest distance, thus calling for more studies for better understanding of
14 Helsinki's ABL processes affected by a range of surfaces. The examples in this paper have highlighted,
15 for example: negative sensible heat fluxes over a city center with very low vegetation fraction, the
16 applicability of urban scintillometry, applying scanning lidar over a city, and the combination of sodar
17 and lidar to give a fuller range of ABL depth estimates. There is also strong indication of the important
18 role of the snow cover in the heat balance over the city. Previous studies in Helsinki have already
19 reported many findings, such as analyses of fluxes (Vesala et al. 2008), exploitation of morphological
20 datasets (Nordbo et al. 2012a), analysis of several years' CO₂ fluxes (Järvi et al. 2012), and air-quality
21 observations (www.airquality.fi, Pirjola et al. 2012).

22 These results will hopefully trigger modeling activities to distinguish and prioritize the various processes
23 at hand. Beyond the forthcoming science outputs, we expect to expand this network. We anticipate that
24 others will bring their equipment and/or expertise alongside ours for the development of technology,
25 science, and applications.

1 **ACKNOWLEDGMENTS**

2 EC FP7 ERC Grant 227915 “Atmospheric planetary boundary layers – physics, modelling and role in
3 Earth system” and Academy of Finland (Project numbers 138328, 1118615 and ICOS-Finland, 263149)
4 provided financial support. Kari Riikonen, Erkki Siivola, Pasi Aalto, and Petri Keronen provided
5 technical support; Kari Niemelä extracted AMDAR data (online supplemental materials); we had useful
6 discussions with Iolanda Iolongo, Mari Kauhaniemi, Juuso Suomi, Jukka Käyhkö, Anu Kousa, Tarja
7 Koskentalo, Heikki Turtiainen, Mikko Laakso, Reijo Roininen, Antti Hellsten, Adriaan Perrels, Mika
8 Komppula, Elena Saltikoff, and Sue Grimmond. We are very grateful for the insightful and
9 constructive comments from the reviewers.

1 **REFERENCES.**

- 2 Allwine, K. J., and J. E. Flaherty, 2006: Joint Urban 2003: Study overview and instrument locations.
3 *PNNL-15967, Pacific Northwest National Laboratory, Richland, WA.*
- 4 Althausen, D., R. Engelmann, H. Baars, B. Heese, A. Ansmann, D. Müller, and M. Komppula, 2009:
5 Portable Raman Lidar Polly XT for Automated Profiling of Aerosol Backscatter, Extinction, and
6 Depolarization. *J. Atmos. Oceanic Technol.*, **26**, 2366–2378.
- 7 Aubinet, M., T. Vesala, and D. Papale, 2012: *Eddy Covariance - A Practical Guide to Measurement and Data*
8 *Analysis*. Springer atmospheric sciences, ISBN13:978-9400723504.
- 9 Barlow, J. F., T. M. Dunbar, E. G. Nemitz, C. R. Wood, M. W. Gallagher, F. Davies, E. O'Connor, and
10 R. M. Harrison, 2011: Boundary layer dynamics over London, UK, as observed using Doppler
11 lidar during REPARTEE-II. *Atmos. Chem. Phys.*, **11**, 2111–2125.
- 12 Bergeron, O., and I. B. Strachan, 2012: Wintertime radiation and energy budget along an urbanization
13 gradient in Montreal, Canada. *Int. J. Climatol.*, **32**, 137–152.
- 14 Changnon, S. A., F. A. Huff, and R. G. Semonin, 1971: METROMEX: an Investigation of Inadvertent
15 Weather Modification. *Bull. Amer. Meteor. Soc.*, **52**, 958–968.
- 16 Collier, C. G. and Coauthors, 2005: Dual-Doppler Lidar Measurements for Improving Dispersion
17 Models. *Bull. Amer. Meteor. Soc.*, **86**, 825–838.
- 18 Cros, B. and Coauthors, 2004: The ESCOMPTE program: an overview. *Atmos. Res.*, **69**, 241–279.
- 19 Eresmaa, N., A. Karppinen, S. M. Joffre, J. Räsänen, and H. Talvitie, 2006: Mixing height determination
20 by ceilometer. *Atmos. Chem. Phys.*, **6**, 1485–1493.
- 21 Eresmaa, N., J. Härkönen, S. M. Joffre, D. M. Schultz, A. Karppinen, and J. Kukkonen, 2012: A three-
22 step method for estimating the mixing height using ceilometer data from the Helsinki Testbed. *J.*
23 *Climate Appl. Meteor.*, **51**, 2172–2187.
- 24 Fisher, B., S. Joffre, J. Kukkonen, M. Piringer, M. Rotach, and M. Schatzmann, 2005: *Meteorology applied*
25 *to Urban Air Pollution Problems, Final Report COST Action 715*. Demetra, Bulgaria, ISBN 954-9526-
26 30-5.
- 27 Grimmond, C.S.B., H. A. Cleugh, and T. R. Oke, 1991: An Objective urban heat storage model and its
28 comparison with other schemes. *Atmos. Environ.* **25B**, 311–326.
- 29 Grimmond, C. S. B., 2006: Progress in measuring and observing the urban atmosphere. *Theor. Appl.*
30 *Clim.*, **84**, 3–22.
- 31 Hanna, S. R. and Coauthors, 2006: Detailed Simulations of Atmospheric Flow and Dispersion in
32 Downtown Manhattan: An Application of Five Computational Fluid Dynamics Models. *Bull.*
33 *Amer. Meteor. Soc.*, **87**, 1713–1726.

- 1 Harrison, R. M. and Coauthors, 2012: Atmospheric chemistry and physics in the atmosphere of a
2 developed megacity (London): an overview of the REPARTEE experiment and its conclusions.
3 *Atmos. Chem. Phys.*, **12**, 3065–3114.
- 4 Hill, R. J., and G. R. Ochs, 1978: Fine calibration of large-aperture optical scintillometers and an optical
5 estimate of inner scale of turbulence. *Appl. Opt.*, **17**, 3608.
- 6 Hirsikko, A. and Coauthors, 2013: Characterising the effect of a variety of surface roughness on
7 boundary layer wind and dynamics within the scanning Doppler lidar network in Finland.
8 European Geophysical Union conference, Vienna, April 2013. EGU2013-8378
- 9 HSY, 2008: Seutu CD – a dataset by the Helsinki Region Environmental Services Authority.
- 10 Hussein, T. and Coauthors, 2008: Observation of regional new particle formation in the urban
11 atmosphere. *Tellus B*, **60**, 509–521.
- 12 Illingworth, A. J. and Coauthors, 2007: Cloudnet. *Bull. Amer. Meteor. Soc.*, **88**, 883–898.
- 13 Järvi, L. and Coauthors, 2009a: Annual particle flux observations over a heterogeneous urban area.
14 *Atmos. Chem. Phys.*, **9**, 7847–7856.
- 15 Järvi, L. and Coauthors, 2009b: The urban measurement station SMEAR III: Continuous monitoring
16 of air pollution and surface-atmosphere interactions in Helsinki, Finland. *Bor. Environ. Res.*, **14**, 86–
17 109.
- 18 Järvi, L. and Coauthors, 2009c: Comparison of net CO₂ fluxes measured with open- and closed-path
19 infrared gas analyzers in an urban complex environment. *Bor. Environ. Res.*, **14**, 499–514.
- 20 Järvi, L., I. Mammarella, W. Eugster, A. Ibrom, E. Siivola, E. Dellwik, P. Keronen, and G. Burba,
21 2009d: Comparison of net CO₂ fluxes measured with open- and closed-path infrared gas
22 analyzers in an urban complex environment. *Bor. Environ. Res.*, **6095**, 499–514.
- 23 Järvi, L., A. Nordbo, H. Junninen, A. Riikonen, J. Moilanen, E. Nikinmaa, and T. Vesala, 2012:
24 Seasonal and annual variation of carbon dioxide surface fluxes in Helsinki, Finland, in 2006–2010.
25 *Atmos. Chem. Phys.*, **12**, 8475–8489.
- 26 Kay, R., and J. Alder, 2005: *Coastal Planning and Management*. 2nd Edition. Taylor and Francis, Abingdon,
27 UK.
- 28 Kipp and Zonen, 2005: *Large aperture scintillometer instruction manual*. Delft, The Netherlands.
- 29 Koskinen, J. T. and Coauthors, 2011: The Helsinki Testbed: A Mesoscale Measurement, Research, and
30 Service Platform. *Bull. Amer. Meteor. Soc.*, **92**, 325–342.
- 31 Kouznetsov, R. D., 2007: Latán-3 sodar for investigation of the atmospheric boundary layer. *Atmos.*
32 *Oceanic Opti.*, **20**, 684–687.
- 33 Kouznetsov, R. D., 2009: The multiple-frequency sodar with high temporal resolution. *Meteor. Z.*, **18**,
34 163–167.

- 1 Kouznetsov, R. D., and M. Kallistratova, 2010: Anisotropy of a small-scale turbulence in the
2 atmospheric boundary layer and its effect on acoustic backscattering. *International Symposium for the*
3 *Advancement of Boundary Layer Remote Sensing, Paris, 28-30 June 2010.*
- 4 Kukkonen, J. and Coauthors, 2005: Analysis and evaluation of selected local-scale PM air pollution
5 episodes in four European cities: Helsinki, London, Milan and Oslo. *Atmos. Environ.*, **39**, 2759–
6 2773.
- 7 Kukkonen, J. and Coauthors, 2012: A review of operational, regional-scale, chemical weather
8 forecasting models in Europe. *Atmos. Chem. Phys.*, **12**, 1–87.
- 9 Kupiainen K. and Coauthors, 2011: Street dust emissions in Finnish cities – summary of results from
10 2006–2010. City of Helsinki Environment Centre 5/2011. Lemonsu, A. and Coauthors, 2008:
11 Overview and first results of the Montreal urban snow experiment 2005. *J. Climate Appl. Meteor.*, **47**, 59–
12 75.
- 13 Lemonsu, A. and Coauthors, 2010: Evaluation of the town energy balance model in cold and snowy
14 conditions during the Montreal urban snow experiment 2005. *J. Climate Appl. Meteor.*, **49**, 346–362.
- 15 Lowry, W. P., 1977: Empirical estimation of urban effects on climate: a problem analysis. *J. Appl.*
16 *Meteor.*, **16**, 129–135.
- 17 Masson, V., 2000: A physically-based scheme for the urban energy budget in atmospheric models.
18 *Bound.-Layer Meteor.*, **94**, 357–397.
- 19 Masson, V. and Coauthors, 2008: The Canopy and Aerosol Particles Interactions in TOulouse Urban
20 Layer (CAPITOUL) experiment. *Meteor. Atmos. Phys.*, **102**, 135–157.
- 21 Mestayer, P. G. and Coauthors, 2005: The urban boundary-layer field campaign in Marseille
22 (UBL/CLU-ESCOMPTE): set-up and first results. *Bound.-Layer Meteor.*, **114**, 315–365.
- 23 Moene, A. F., O. K. Hartogensis, and F. Beyrich, 2009: Developments in Scintillometry. *Bull. Amer.*
24 *Meteor. Soc.*, **90**, 694–698.
- 25 Mårtensson, E. M., E. D. Nilsson, G. Buzorius, and C. Johansson, 2006: Eddy covariance
26 measurements and parameterisation of traffic related particle emissions in an urban environment.
27 *Atmos. Chem. Phys.*, **6**, 769–785.
- 28 Nordbo, A., L. Järvi, S. Haapanala, J. Moilanen, and T. Vesala, 2012a: Intra-city variation in urban
29 morphology and turbulence structure in Helsinki, Finland. *Bound.-Layer Meteor.*,
30 doi:10.1007/s10546-012-9759-9.
- 31 Nordbo, A., L. Järvi, S. Haapanala, C. R. Wood, and T. Vesala, 2012b: Fraction of natural area as main
32 predictor of net CO₂ emissions from cities. *Geophys. Res. Lett.*, **39**, L20802.
- 33 Nordbo, A., L. Järvi, and T. Vesala, 2012c: Revised eddy covariance flux calculation methodologies –
34 effect on urban energy balance. *Tellus Ser. B-Chem. Phys. Meteorol.*, **64**, 18184.
- 35 O'Connor, E. J., A. J. Illingworth, and R. J. Hogan, 2004: A Technique for Autocalibration of Cloud
36 Lidar. *J. Atmos. Oceanic Technol.*, **21**, 777–786.

- 1 Oke, T. R., 1987: *Boundary Layer Climates*. Routledge, London, UK.
- 2 Pearson, G., F. Davies, and C. Collier, 2009: An Analysis of the Performance of the UFAM Pulsed
3 Doppler Lidar for Observing the Boundary Layer. *J. Atmos. Oceanic Technol.*, **26**, 240–250.
- 4 Pirinen, P., H. Simola, J. Aalto, J.-P. Kaukoranta, P. Karlsson, and R. Ruuhela, 2012: *Climatological*
5 *Statistics of Finland 1981–2010*. Finnish Meteorological Institute, Reports, No. 2012:1.
- 6 Pirjola, L. and Coauthors, 2012: Spatial and temporal characterization of traffic emissions in urban
7 microenvironments with a mobile laboratory. *Atmos. Environ.*, **63**, 156–167.
- 8 Population Register Center of Finland, 2012: “Population by municipality as of 31 January 2012” (in Finnish
9 and Swedish). *Population Information System*. Retrieved 16 February 2012.
- 10 Ripamonti G., L. Järvi, B. Mølgaard, T. Hussein, A. Nordbo, and K. Hämeri, 2013: The effect of
11 local sources on aerosol particle number size distribution, concentrations and fluxes in
12 Helsinki, Finland. *In review in Tellus B*.
- 13 Rotach, M. W., B. Fisher, and M. Piringer, 2002: COST 715 workshop on urban boundary layer
14 parameterizations. *Bull. Amer. Meteor. Soc.*, **83**, 1501–1504.
- 15 Rotach, M. W. L. and Coauthors, 2005: BUBBLE - An urban boundary layer meteorology project.
16 *Theoretical and applied climatology*. *Wien, New York NY*, **81**, 261.
- 17 Roth, M., 2000: Review of atmospheric turbulence over cities. *Quart. J. Roy. Meteor. Soc.*, **126**, 941–990.
- 18 Saarnio, K., K. Teinilä, M. Aurela, H. Timonen, and R. Hillamo, 2010: High-performance anion-
19 exchange chromatography-mass spectrometry method for determination of levoglucosan,
20 mannosan, and galactosan in atmospheric fine particulate matter. *Anal. Bioanal. Chem.*, **398**, 2253–
21 2264.
- 22 Sailor, D. J., 2011: A review of methods for estimating anthropogenic heat and moisture emissions in
23 the urban environment. *Int. J. Climatol.* **31**, 189–299.
- 24 Schneider, A., M. A. Friedl, and D. Potere, 2009: A new map of global urban extent from MODIS
25 satellite data. *Environ. Res. Lett.*, **4**, 44003.
- 26 Suni, T. and Coauthors, 2003: Long-term measurements of surface fluxes above a Scots pine forest in
27 Hyytiälä, southern Finland, 1996–2001. *Bor. Environ. Res.*, **8**, 287–301.
- 28 Suomi, I., 2004: Fog over the Gulf of Finland on 8 September, 2002 (In Finnish). MSc thesis,
29 University of Helsinki, 54 pp.
- 30 Tammelin, B. and Coauthors, 2012: Production of the Finnish Wind Atlas. *Wind Energy*, **16**, 19–35.
- 31 Uijlenhoet, R., J.-M. Cohard, and M. Gosset, 2011: Path-Average Rainfall Estimation from Optical
32 Extinction Measurements Using a Large-Aperture Scintillometer. *J. Hydrometeorol.*, **12**, 955–972.
- 33 Vesala, T. and Coauthors, 2008: Surface–atmosphere interactions over complex urban terrain in
34 Helsinki, Finland. *Tellus B*, **60**, 188–199.

- 1 Vihma, T., and B. Brümmer, 2002: Observations and modelling of on-ice and off-ice flows in the
2 northern Baltic Sea. *Bound.-Layer Meteor.*, **103**, 1–27.
- 3 Wood, C. R. and Coauthors, 2009: Dispersion Experiments in Central London: The 2007 DAPPLE
4 project. *Bull. Amer. Meteor. Soc.*, **90**, 955–969.
- 5 Wood, C. R. and Coauthors, 2010: Turbulent flow at 190 m height above London during 2006–2008: A
6 climatology and the applicability of similarity theory. *Bound.-Layer Meteor.*, **137**, 77–96.
- 7 Wood, C. R., R. D. Kouznetsov, and A. Karppinen, 2012: An automatic algorithm for detecting
8 mixing-height from SODAR. *International Symposium for the Advancement of Boundary Layer Remote
9 Sensing. Colorado, June 2012*, 102–105.
- 10 Wood, C. R., R. D. Kouznetsov, R. Gierens, A. Nordbo, L. Järvi, M. A. Kallistratova, and J. Kukkonen,
11 2013a: The structure parameter for temperature over Helsinki from sonic anemometry and
12 scintillometry. *J. Atmos. Oceanic Technol.*, Re-submitted.
- 13 Wood, C. R., L. Pauscher, S. Kotthaus, J. F. Barlow, H. Ward, S. Lane, and S. Grimmond, 2013b: Wind
14 observations over the River Thames in central London. *Sci. Total Environ.*, **442**, 527–533.
- 15 Zeweldi, D. A., M. Gebremichael, J. Wang, T. Sammis, J. Kleissl, and D. Miller, 2009: Intercomparison
16 of Sensible Heat Flux from Large Aperture Scintillometer and Eddy Covariance Methods: Field
17 Experiment over a Homogeneous Semi-arid Region. *Bound.-Layer Meteor.*, **135**, 151–159.
- 18

1 **FIGURE CAPTIONS.**

2 **FIG. 1. Maps of Helsinki with equipment locations marked. (a) Shown are profile masts at**
3 **Kivenlahti and Isosaari island, Vaisala site, and airport. The extent of the area shown in a is**
4 **approximately 38km longitude by 38km latitude. The red box shows the area in subplot b. (b)**
5 **Land-use map: urban/paved (white), vegetative (green), water (blue); (HSY 2008). The sodar**
6 **moved from Kumpula westward to Pasila. The grid-points of the HARMONIE model are 2.5**
7 **km spacing on Lambert conformal plane (see online supplemental materials).**

8 **FIG. 2. Median monthly (a) net all-wave radiation, and (b) upwelling shortwave radiation; for**
9 **2011 at Kumpula and downtown (Torni) calculated for times that are daytime throughout the**
10 **year (08:00–12:00 hours UTC). The error bars show quartile deviations during the plotted**
11 **hours.**

12 **FIG. 3. Mean sensible heat flux for each 30-min period for each month of 2011 at (a) Kumpula,**
13 **(b) downtown (Torni), and (c) their difference (same color scales in all subplots). Sunrise and**
14 **sunset times are shown as thick dashed black line. Zero sensible heat flux is shown as white**
15 **line. For all 30-min periods in 2011, negative sensible heat fluxes occurred 48% of the time at**
16 **Kumpula and 13% downtown (Torni).**

17 **FIG. 4. Conditions in Helsinki on 4th September 2011, at Kumpula (black) and downtown**
18 **(Torni, red) for: (a) net all-wave radiation, (b) wind speed, (c) short-wave radiation, (d) wind**
19 **direction, (e) long-wave radiation, and (f) Kumpula pressure (blue) and relative humidity**
20 **(green). Upwelling and downwelling radiation is marked with dashed (- -) and solid (-) lines**
21 **respectively.**

22 **FIG. 5. Camera view (red circle in a) westward from Fire Station mast over downtown: (a)**
23 **photograph taken 5th April 2011, with red-brick Fire Station tower in foreground; (b) thermal**

1 camera images at 10:20 hours UTC (solar noon); and (c) 21:00 on 4th September 2011. The
2 camera is centered so that the horizon equally bisects the image at the center.

3 FIG. 6. Variance of vertical velocity ($\text{m}^2 \text{s}^{-2}$) in Kumpula on 4th September 2011 from (a) sodar
4 and (b) lidar; the same color scale for both plots. The sodar's 400-meter range is marked also
5 on the lidar panel (black line), easing comparison. The red line in a is the ABL depth
6 estimated from sodar acoustic backscatter (Wood et al. 2012).

7 FIG. 7. Time series of (a) sensible heat flux and (b) structure parameter of temperature (C_T^2) on
8 4th September 2011. The city-scale scintillometer is from downtown (Torni) to Kumpula. Eddy-
9 covariance data with thick lines and markers have stringent quality assurance, such as flux
10 non-stationarity and mast interference (Nordbo et al. 2012a); lighter-dashed lines have less-
11 stringent quality assurance.

12 FIG. 8. Time series on 3rd January 2012 of (a) sensible heat flux, and (b) Monin-Obukhov
13 stability parameter at Kumpula (black) and downtown (Torni, red), (c) turbulent kinetic
14 energy budget at Kumpula, (d) particle flux at Kumpula, and (e) particle concentration at
15 Kumpula. Data with thick lines and x-markers in a,b,d,e have stringent quality assurance, such
16 as flux non-stationarity and mast interference (Nordbo et al. 2012a); lighter-dashed lines have
17 less-stringent quality assurance. The transport term in c is calculated as the residual of the
18 other terms: time derivative of turbulent kinetic energy (black square), shear production in the
19 streamwise (blue circle) and crosswind (blue dot) directions, buoyancy (red squares), and
20 dissipation (black crosses).

21 FIG. 9. Vertical profiles from lidar at Kumpula on 3rd January 2012. (a) Lidar backscatter values
22 of 10^{-7} to 5×10^{-6} are typically aerosol (blue and green), whilst values above 10^{-5} are cloud
23 droplets (red). (b) Variance of vertical velocity, with 30-min mean threshold of $0.1 \text{ m}^2 \text{ s}^{-2}$ (red)
24 as a crude ABL depth estimator.

1 **FIG. 10. Comparison of 30-min mean northward (v) component horizontal winds from sonic**
2 **anemometer at Kumpula and downtown (Torni) with lidar beam pointing from Kumpula due**
3 **south (range-gate 4: 90–120 m) on 3rd January 2012. Statistics between lidar and sonic**
4 **anemometer at Kumpula from the 30-min data on this day are: correlation coefficient 0.96,**
5 **root-mean-square difference 0.52 m s^{-1} , and bias -0.32 m s^{-1} (sonic anemometer greater than**
6 **lidar).**

7

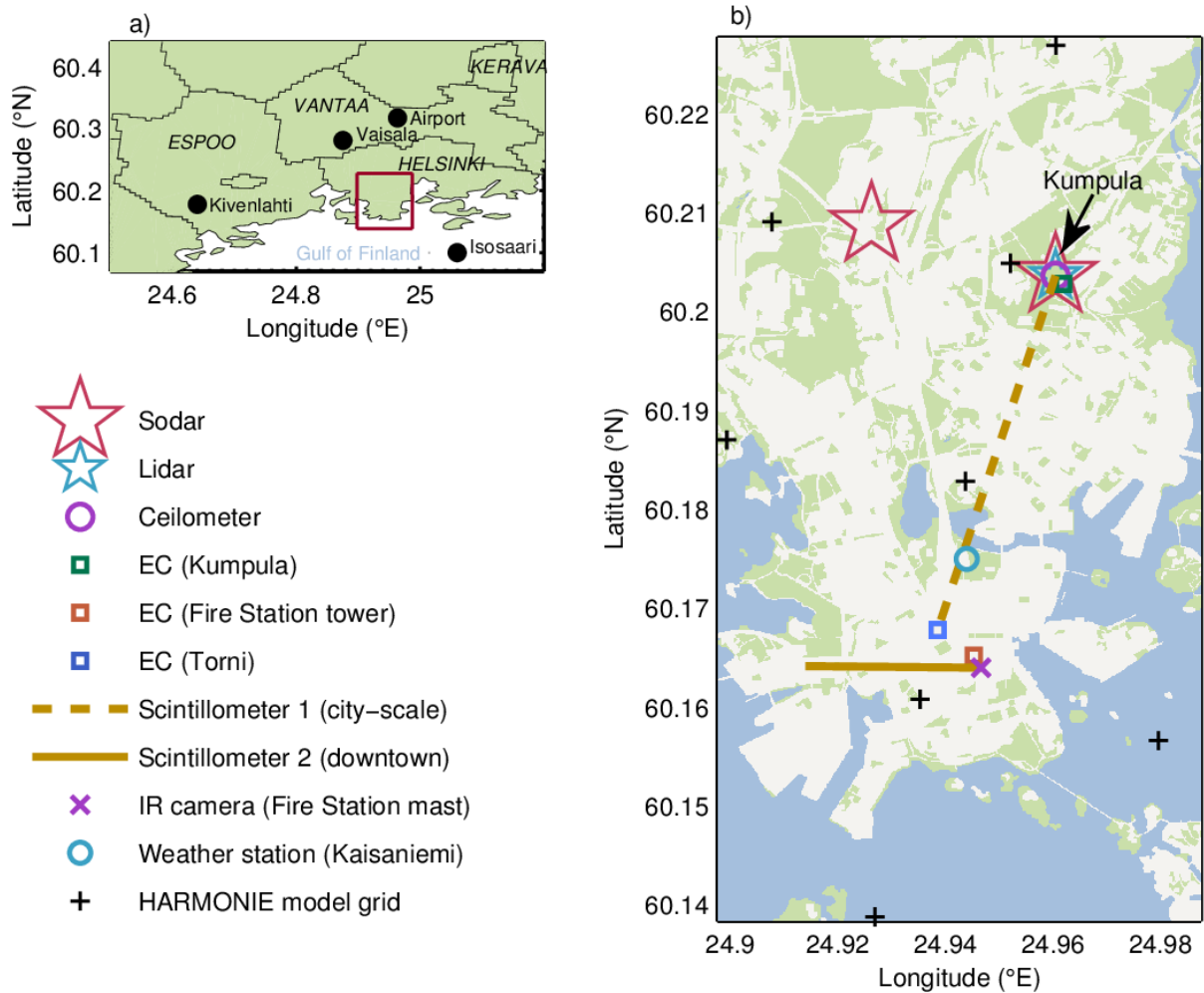
8

9 **TABLES**

TABLE 1. List of the core equipment, their locations (latitude, longitude), and uses. (EC = eddy covariance, ABL = atmospheric boundary layer)

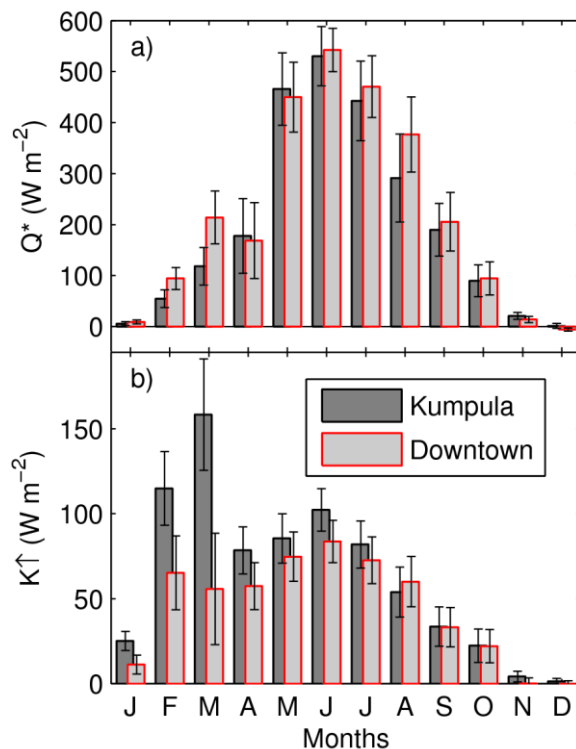
Instrument	Location	Founding year	Measurement	Important derived variables	Details
Sodar	Kumpula (60.202817°N 24.961128°E) Pasila (60.208800°N 24.926300°E)	2009	Acoustic backscatter profile	ABL depth, profiles of mean and variance of vertical velocity	(Wood et al. 2012)
Lidar	Kumpula (60.203644°N 24.960525°E)	2011	Doppler velocity and aerosol backscatter	ABL depth, profiles of vertical velocity variance, and aerosol backscatter	(Hirsikko et al. 2013)
Ceilometer	Kumpula (60.203644°N 24.960525°E)	2009	Aerosol backscatter	ABL depth	(Eresmaa et al. 2006, 2012)
EC SMEAR-III	Kumpula (60.202817°N 24.961128°E)	2004	Sonic anemometry Infra-red gas analyzer	Fluxes, turbulence statistics, and mean concentrations of heat, moisture, momentum, and carbon dioxide	(Vesala et al. 2008; Järvi et al. 2009c)
EC Fire Station	Downtown (60.165211°N 24.945356°E)	2010	"	"	(Nordbo et al. 2012a)
EC Tornio	Downtown (60.167803°N 24.938600°E)	2010	"	"	"
Scintillometer 1	Tornio→Kumpula, city-scale(60.167803–60.2036444°N 24.938600–24.960525°E)	2011	Structure parameter of temperature	Sensible heat flux, wind speed	(Wood et al. 2013a)
Scintillometer 2	Fire Station mast→Sitra, downtown (60.164000–60.164158°N 24.946667–24.9140111°E)	2012	"	"	"
Infra-red camera	Fire Station mast, downtown (60.164000°N 24.946667°E)	2010	Brightness temperature	–	–

1 **FIGURES.** (In this .doc file are low-quality png's; also uploaded are eps and pdf files)



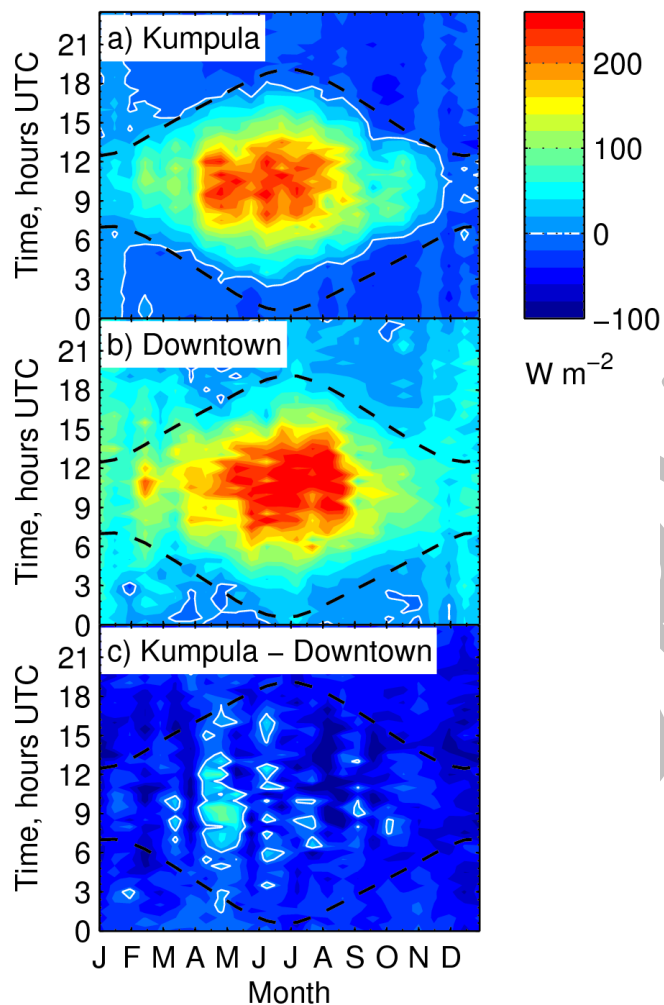
2

3 **FIG. 1. Maps of Helsinki with equipment locations marked. (a)** Shown are profile
4 masts at Kivenlahti and Isosaari island, Vaisala site, and airport. The extent of the area
5 shown in a is approximately 38km longitude by 38km latitude. The red box shows the
6 area in subplot b. (b) Land-use map: urban/paved (white), vegetative (green), water
7 (blue); (HSY 2008). The sodar moved from Kumpula westward to Pasila. The grid-points
8 of the HARMONIE model are 2.5 km spacing on Lambert conformal plane (see online
9 supplemental materials).



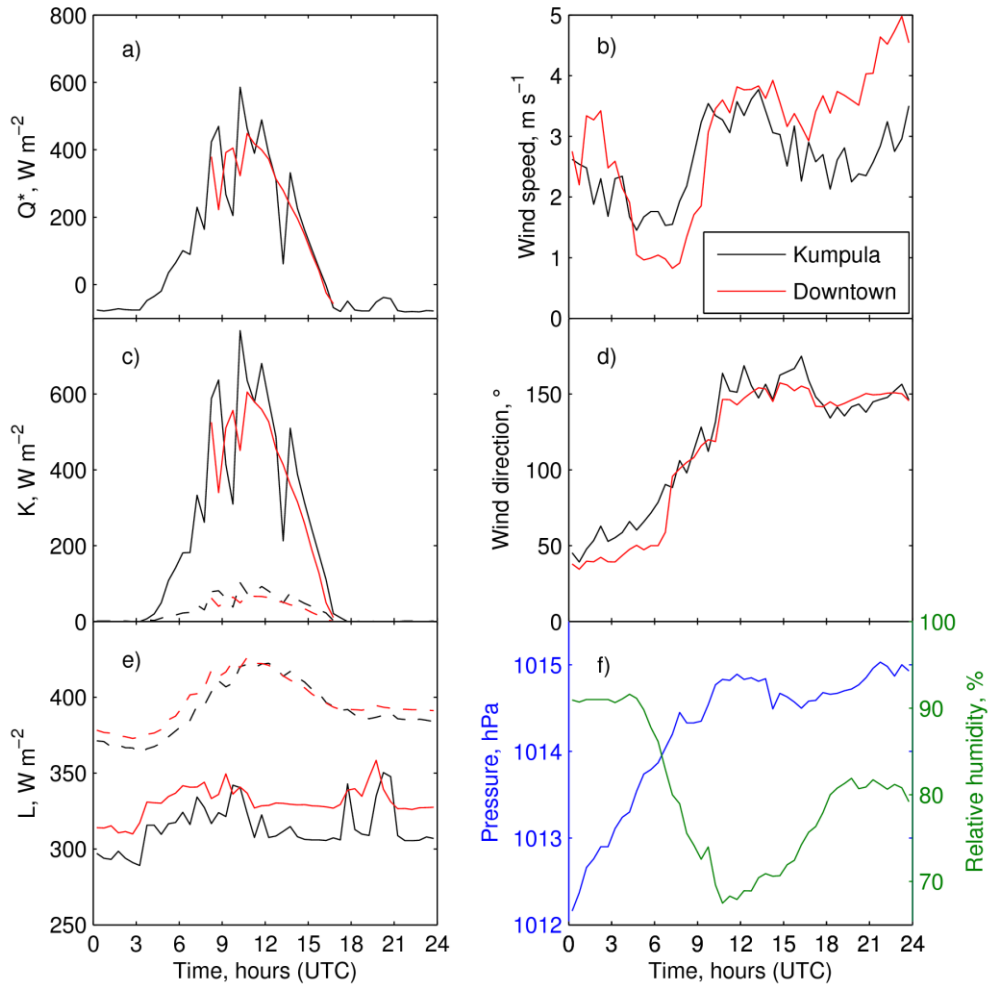
1
2
3
4
5
6

FIG. 2. Median monthly (a) net all-wave radiation, and (b) upwelling shortwave radiation; for 2011 at Kumpula and downtown (Torni) calculated for times that are daytime throughout the year (08:00–12:00 hours UTC). The error bars show quartile deviations during the plotted hours.



1
2
3
4
5
6
7

FIG. 3. Mean sensible heat flux for each 30-min period for each month of 2011 at (a) Kumpula, (b) downtown (Torni), and (c) their difference (same color scales in all subplots). Sunrise and sunset times are shown as thick dashed black line. Zero sensible heat flux is shown as white line. For all 30-min periods in 2011, negative sensible heat fluxes occurred 48% of the time at Kumpula and 13% downtown (Torni).



1

2

3

4

5

6

7

FIG. 4. Conditions in Helsinki on 4th September 2011, at Kumpula (black) and downtown (Torni, red) for: (a) net all-wave radiation, (b) wind speed, (c) short-wave radiation, (d) wind direction, (e) long-wave radiation, and (f) Kumpula pressure (blue) and relative humidity (green). Upwelling and downwelling radiation is marked with dashed (- -) and solid (-) lines respectively.

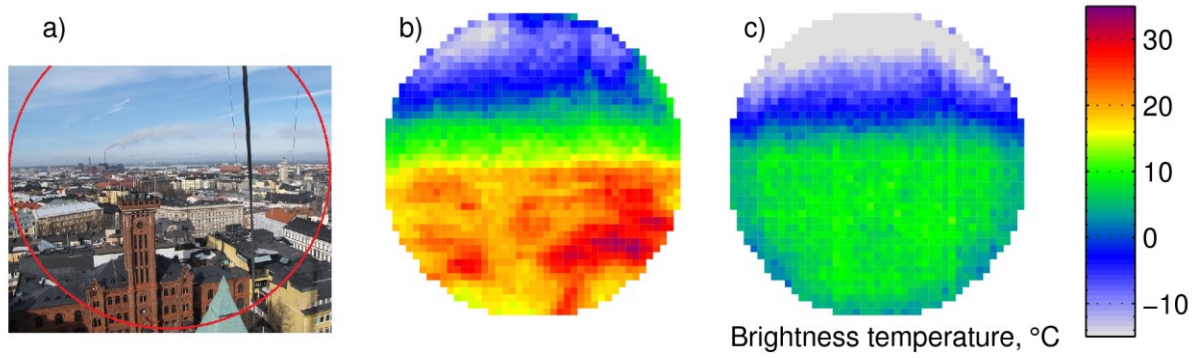
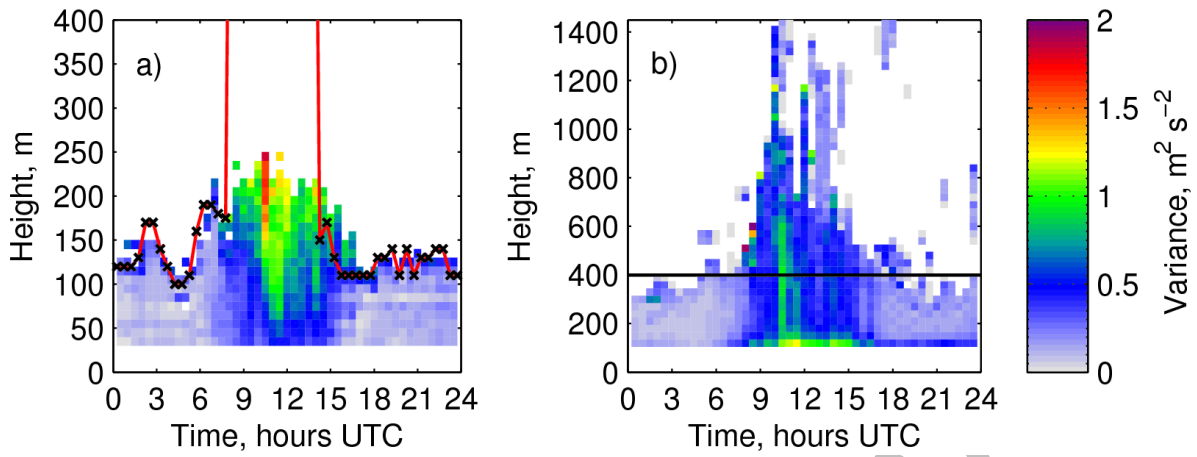
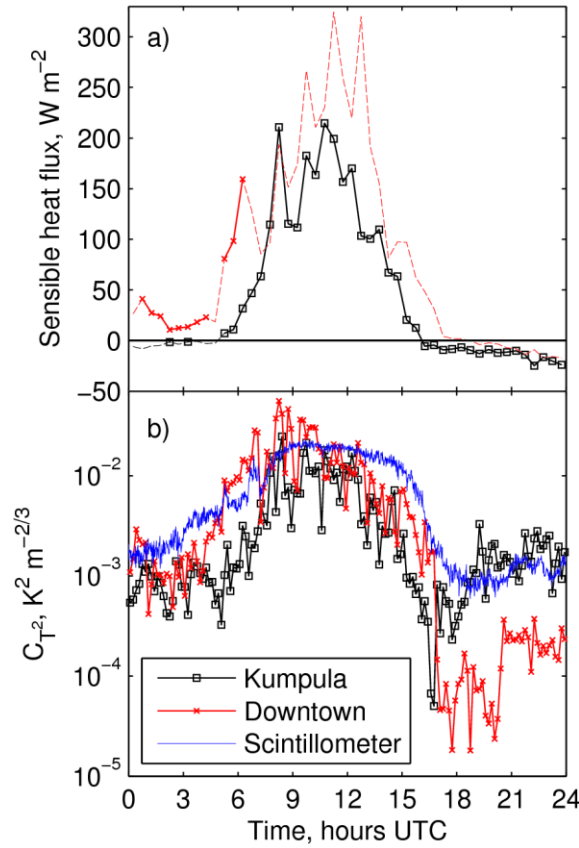


FIG. 5. Camera view (red circle in a) westward from Fire Station mast over downtown: (a) photograph taken 5th April 2011, with red-brick Fire Station tower in foreground; (b) thermal camera images at 10:20 hours UTC (solar noon); and (c) 21:00 on 4th September 2011. The camera is centered so that the horizon equally bisects the image at the center.

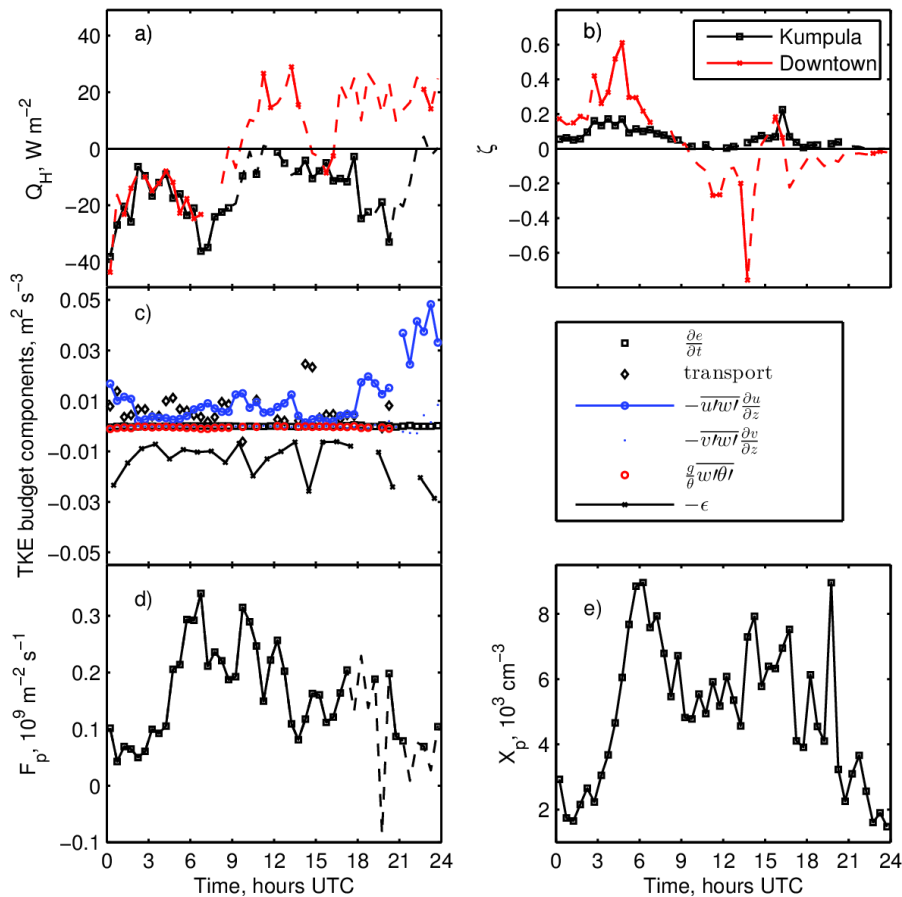


1
2 **FIG. 6. Variance of vertical velocity ($\text{m}^2 \text{s}^{-2}$) in Kumpula on 4th September 2011 from**
3 **(a) sodar and (b) lidar; the same color scale for both plots. The sodar's 400-meter range is**
4 **marked also on the lidar panel (black line), easing comparison. The red line in a is the**
5 **ABL depth estimated from sodar acoustic backscatter (Wood et al. 2012).**
6



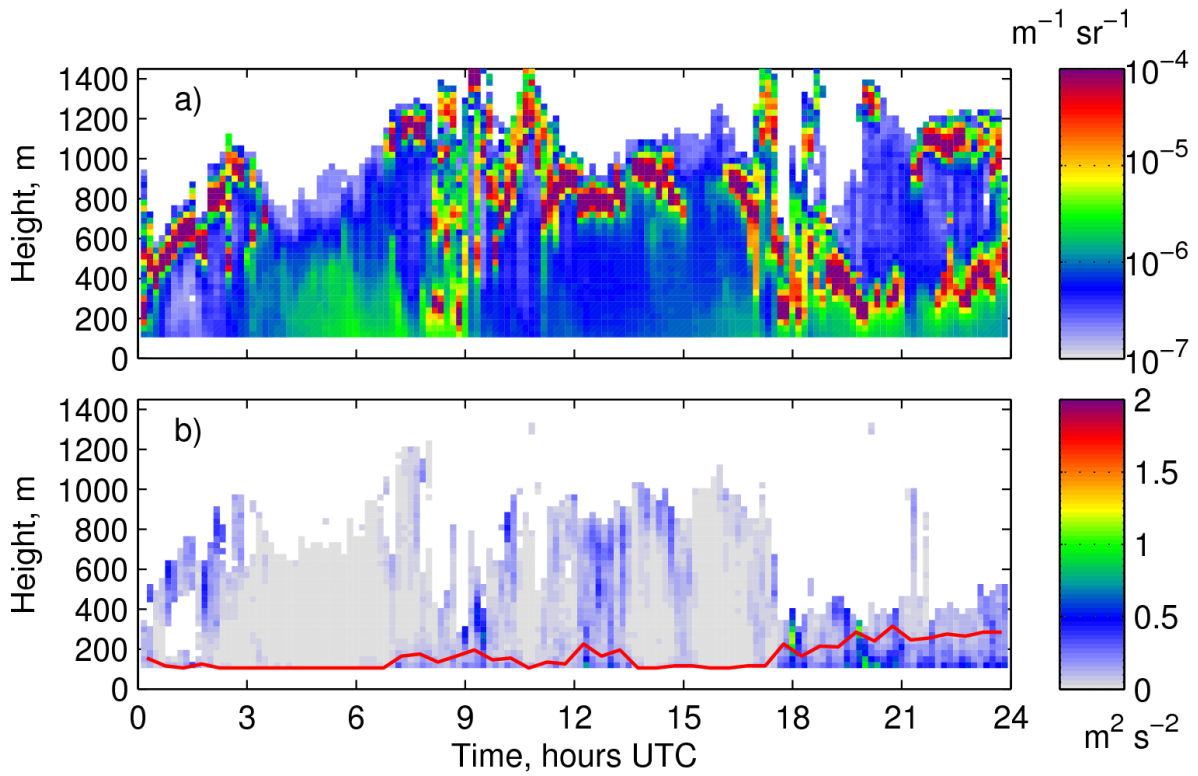
1
2
3
4
5
6
7
8

FIG. 7. Time series of (a) sensible heat flux and (b) structure parameter of temperature (C_T^2) on 4th September 2011. The city-scale scintillometer is from downtown (Torni) to Kumpula. Eddy-covariance data with thick lines and markers have stringent quality assurance, such as flux non-stationarity and mast interference (Nordbo et al. 2012a); lighter-dashed lines have less-stringent quality assurance.



1
 2 **FIG. 8.** Time series on 3rd January 2012 of (a) sensible heat flux, and (b) Monin-
 3 Obukhov stability parameter at Kumpula (black) and downtown (Torni, red), (c)
 4 turbulent kinetic energy budget at Kumpula, (d) particle flux at Kumpula, and (e) particle
 5 concentration at Kumpula. Data with thick lines and x-markers in a,b,d,e have stringent
 6 quality assurance, such as flux non-stationarity and mast interference (Nordbo et al.
 7 2012a); lighter-dashed lines have less-stringent quality assurance. The transport term in c
 8 is calculated as the residual of the other terms: time derivative of turbulent kinetic energy
 9 (black square), shear production in the streamwise (blue circle) and crosswind (blue dot)
 10 directions, buoyancy (red squares), and dissipation (black crosses).

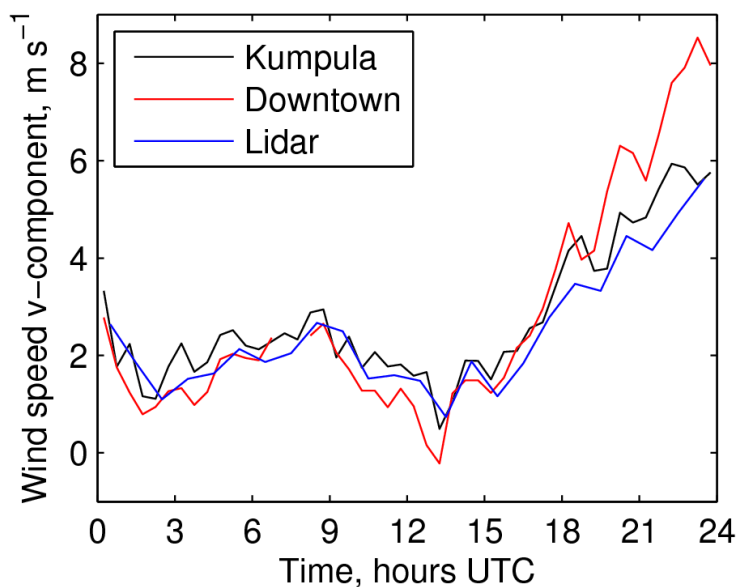
1



2

3 **FIG. 9. Vertical profiles from lidar at Kumpula on 3rd January 2012. (a) Lidar**
 4 **backscatter values of 10^{-7} to 5×10^{-6} are typically aerosol (blue and green), whilst values**
 5 **above 10^{-5} are cloud droplets (red). (b) Variance of vertical velocity, with 30-min mean**
 6 **threshold of $0.1 \text{ m}^2 \text{ s}^{-2}$ (red) as a crude ABL depth estimator.**

7



1

2 **FIG. 10. Comparison of 30-min mean northward (v) component horizontal winds**
3 **from sonic anemometer at Kumpula and downtown (Torni) with lidar beam pointing**
4 **from Kumpula due south (range-gate 4: 90–120 m) on 3rd January 2012. Statistics between**
5 **lidar and sonic anemometer at Kumpula from the 30-min data on this day are: correlation**
6 **coefficient 0.96, root-mean-square difference 0.52 m s⁻¹, and bias -0.32 m s⁻¹ (sonic**
7 **anemometer greater than lidar).**

8

1 Online Supplemental Material for:

2 “An overview on the Urban Boundary-layer

3 Atmosphere Network in Helsinki”

4 Wood CR et al.

5 **Further technical characteristics of core measurements**

6 In addition to Table 1 in the main text, we supply here further technical details of core

7 measurements.

8 **Table S1 – technical details of instruments mentioned in main text.**

Instrument	Manufacturer
CNR4	Kipp&Zonnen, Delft, The Netherlands
SI-111 (radiation thermometers, with 22-degree half-width field of view)	Apogee Instruments Inc., Utah, USA
SI-121 (infra-red radiation sensors, with 18-degree half-width field of view)	Apogee Instruments Inc., Utah, USA
Streamline (scanning doppler lidar)	HALO-Photonics, Malvern, UK
CL31, CL51 (ceilometers)	Vaisala, Vantaa, Finland
BLS900 (scintillometers)	Scintec, Rottenburg, Germany
OSXL-101 (infra-red camera)	Omega, Stamford, CT, USA

1 **Auxiliary Measurements**

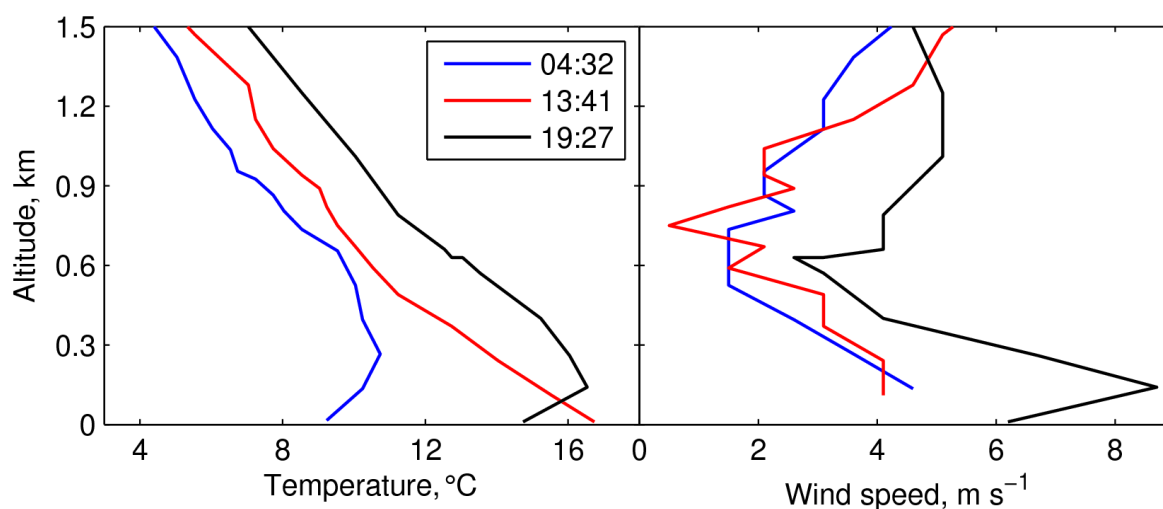
2 Here we review the existence of further observational datasets whose primary purpose was
3 not for the study of Helsinki's atmospheric boundary layer (ABL), but nonetheless will prove
4 useful in future analyses (such as discerning urban versus non-urban effects). Most of the
5 following data are a subset of those available from Helsinki's mesoscale set-up: the Helsinki
6 Testbed (Koskinen et al. 2011).

7 **Soundings**

8 The nearest operational radiosoundings are performed about 100 km north-west of
9 Helsinki at Jokioinen. Occasional soundings are also made from Vaisala premises in Vantaa:
10 approximately 13 km north of downtown Helsinki. The University of Helsinki also has sounding
11 equipment that could be used during intense observation periods from the Kumpula campus.

12 Data from commercial aircraft (Aircraft Meteorological Data Relay, AMDAR) give
13 additional soundings (temperature, wind speed, and direction). From Helsinki–Vantaa airport 14
14 km north of downtown Helsinki, there are 1–9 soundings per day (20–50 per week) covering all
15 times of the day and night. For a given profile, data are available no more frequently than 10
16 second intervals leading to a finest vertical resolution of approximately 70 meters. Unfortunately
17 for Helsinki UrBAN, most flights do not head directly southwards over downtown Helsinki.
18 Nonetheless, at a height of 1 km most planes have travelled only 8–10 km horizontally, which
19 will mean that some planes will give useful ABL information over some of the Helsinki
20 Metropolitan area, whilst other planes will sample the incoming/outgoing air north of the
21 Helsinki Metropolitan area. Vertical profiles of wind speed and temperature (Figure S1) were
22 extracted from AMDAR data for the first case study in the main paper. Consistent with clear
23 skies, a temperature inversion was observed for both nights (04:32 and 19:27 hours UTC), and
24 weak super-adiabatic layer during daytime. There is even evidence of a jet at 19:27. Fuller analysis
25 of AMDAR data over many seasons and wind directions will lead to further understanding of the

1 effect of Helsinki on the ABL, perhaps in combination with extra radiosonde releases and/or
 2 mast data.



3
 4 **Figure S1 – Profiles of temperature and wind from aircraft at Helsinki–Vantaa airport**
 5 **(AMDAR data) on the first case study day (4th September 2011), start times (hours UTC)**
 6 **of profiles are shown in the legend (and take 2–5 minutes to complete).**

7 *Weather Masts*

8 There are no very tall structures in Helsinki, perhaps among the taller is 2 km north-west of
 9 downtown: the Olympic Stadium tower (73 m tall, 60.185°N, 24.929°E). It had a weather station
 10 during Testbed years (ca. 2006–2010, see above) and has re-started measurements on August 30,
 11 2012 (Vaisala WXT 520: temperature, wind speed and direction, pressure, humidity, and rainfall).

12 There are two nearby tall profile masts (Rantamäki et al. 2005; Suomi et al. 2012).
 13 Kivenlahti, 15 km east of downtown Helsinki, is a media broadcasting mast equipped (WMO
 14 code 02838) from June 1989 onwards. The distance to the coast is about 5–8 km in eastern and
 15 southern sectors. Wind speed and direction are measured at four levels: 26, 93, 218, and 327
 16 meters (HydroTech WD-2 and WS-2 instruments). Instruments are located on the western side
 17 of the mast, causing mast shadowing effects on the measurements for wind directions 90–140°.
 18 Temperature measurements are available from 8 levels: 5, 26, 48, 93, 141, 218, 266, and 296

1 meters. Relative humidity is observed at two levels: 93 and 327 meters (HMP35, Vaisala Ltd,
2 Vantaa, Finland).

3 Isosaari island, about 8 km southeast of downtown Helsinki, had a mast equipped with
4 instruments by Vaisala in autumn 2008 as a part of the Finnish Wind Atlas project. Although
5 they are not urban measurements, information on the incoming mesoscale and marine flow is of
6 use for many ABL studies. Continuous observations on this mast are available from the end of
7 November 2008 until the beginning of November 2011. Wind speed measurements are made at
8 three levels: 42, 62, and 83 meters (Vaisala WAA151 cup anemometers). Wind direction is
9 recorded at 40 and 81 meters (Vaisala WAV151 wind vanes). Temperature and humidity
10 observations are available from two levels: 42 and 83 m (Vaisala HMP45D sensors).

11 Since Helsinki is located on the coast of the Gulf of Finland, and downtown is located on a
12 peninsula, understanding the sea is important for understanding the climate of Helsinki. A
13 weather mast—such as the one at Isosaari—gives valuable information on the marine ABL, and
14 especially for southerly winds which could be used to understand the structure of internal
15 boundary layers growing over downtown Helsinki. There are also standard WMO meteorological
16 measurements along the coast of the Gulf of Finland, for example on 2 islands offshore Helsinki
17 (Harmaja, 7 km south, and Kirkkonummi Mäkiluoto, 43 km SW from downtown Helsinki,
18 respectively).

19 *Ground-based Radar*

20 The analysis of data from dual-polarization Doppler weather radars can provide
21 information on the 3D structure and temporal evolution of the wind field. Three dual-
22 polarization C-band Doppler weather radars (in Kumpula, Vantaa, and Kerava) are stationed in
23 the Helsinki Metropolitan area (Saltikoff et al., 2011). Those radars form three dual-Doppler pairs
24 with radar spacings of 22 km between Kumpula and Kerava radars, 10 km between Vantaa and
25 Kumpula radar, and 20 km between Vantaa and Kerava radars. This setup provides a rather

1 complete dual-Doppler coverage of the Helsinki Metropolitan area. Assuming a minimum
2 crossing angle of 30° , the retrieved horizontal wind components will have variances of less than
3 two times the variances of single radar Doppler velocity estimates (Davies-Jones 1979). Typically,
4 it is expected that Doppler velocities can be estimated with an error variance of $1 \text{ m}^2 \text{ s}^{-2}$. In an
5 urban area, due to ground clutter contamination of the radar signal, an actual error in the velocity
6 estimate is expected to be somewhat larger. This error depends on the radar signal strength and
7 absolute value of the Doppler velocity.

8 In the current radar schedule, low-level Doppler measurements are carried out twice every
9 15 minutes (Saltikoff and Neuvonen 2011). For dual-Doppler observations, the other two radars
10 use the same scan settings. These scans provide velocity measurements with a maximum
11 unambiguous velocity of 48 m s^{-1} and range resolution 125 meters. The height of the
12 measurements, defined as the height of the center of a radar beam, depends on distance from the
13 radar and varies between roughly 50 and 200 meters above the mean sea level.

14 *Building Databases*

15 Helsinki Region Environmental Services Authority (HSY) provides a comprehensive
16 database (seutuCD) where detailed Helsinki metadata is given. The database includes, for
17 example, the type of surface cover with 10-meter resolution for Helsinki Metropolitan area,
18 detailed information about the building dimensions, population and building materials. In
19 addition, the National Land Survey of Finland (NLS) has conducted laser scanning measurements
20 with 2-meter resolution for Helsinki Metropolitan area in 2008, and this dataset is available to
21 provide detailed information about the building and vegetation dimensions. The databases can be
22 combined together to provide information that can be used to obtain relevant surface
23 quantities—e.g. zero-place displacement height and aerodynamic roughness length (Nordbo et al.
24 2012)—using morphological methods (MacDonald et al. 1998; Grimmond and Oke 1999).

1 *Traffic Data*

2 Traffic monitoring in the Helsinki Metropolitan area is made by the Helsinki City Planning
3 Department (Lilleberg and Hellman 2011). Distinction between light- and heavy-duty vehicles is
4 made using human visual counts. Continuous traffic counts, with 15 minute resolution during
5 rush hours and with hourly resolution outside, are monitored at main roads. The traffic volumes
6 and average travel speeds of each traffic link are computed using EMME/2 transportation
7 planning system (Kauhaniemi et al. 2008). The model allows for the diurnal and daily variations
8 both in traffic volumes and speeds. The closest continuous online monitoring point to Kumpula
9 (a core site in our network, FIG. 1 in main paper) is located about 2.5 km south on Itäväylä
10 highway.

11 *Satellite-borne Remote-sensing*

12 There is no known use of satellite data to understand Helsinki's ABL. But there is certainly
13 potential for mapping temperature using the MODIS satellite (Weng 2009; Tomlinson et al.
14 2012); and of atmospheric composition—the Ozone Monitoring Instrument, OMI, (Levelt et al.
15 2006) could be used for urban air quality applications using tropospheric NO₂ (Boersma et al.
16 2011), O₃ (Kar et al. 2010), SO₂ (Fioletov et al. 2011), NO₂ (De Ruyter de Wildt et al. 2012), and
17 aerosol optical depth (Natunen et al. 2010).

18 **Model Development**

19 Given the variety of observational scales that the network covers, modeling approaches will
20 help to understand the physical processes of Helsinki's ABL. Indeed, we also expect that some
21 models might be improved as a result of analysis of data from Helsinki UrBAN.

22 FMI participates in the development of the HARMONIE numerical weather prediction
23 (NWP) system (HIRLAM-B 2012), which is the main mesoscale numerical forecast suite of FMI.
24 The model is run with a horizontal mesh-size of 2.5 km and 65 terrain-following levels, with the

1 lowest level at approximately 12 m above the surface, and 20 levels in the lowest 1000 m.
2 Parameterizations of sub grid-scale physical processes are the same as in the AROME-model
3 (Seity et al. 2011) including interactions with the surface—taken into account with the
4 autonomous surface-interaction module SURFEX (Le Moigne 2009): describing up to 4 different
5 surface types per grid cell, including vegetated and built-up areas. Characteristics of the surface
6 for NWP are obtained from the global 1-km resolution ECOCLIMAP database (Masson et al.
7 2003).

8 In SURFEX, each tile responds to the same atmospheric forcing at the lowest model level,
9 but is handled by a separate module. For vegetated and built-up surfaces, the forcing is
10 transmitted via the CANOPY surface ABL scheme (Masson and Seity 2009)—where the ABL is
11 resolved prognostically. Urban areas are handled by the Town Energy Balance model, TEB
12 (Masson 2000). Forced by incoming radiation, precipitation, wind speed, air temperature, and
13 humidity above the rooftops, TEB returns the upward radiative and turbulent heat fluxes, as well
14 as the wind, temperature, and humidity within the urban canopy. The energy and water budgets
15 are solved separately for roofs, walls, and roads, taking into account the shading effect of the
16 walls and the radiative heat exchange between the wall and road surfaces. Heat and water vapor
17 released by traffic and industry may be prescribed, and the heating of building space is
18 dynamically modeled by maintaining the inside temperature above a prescribed minimum level.
19 SURFEX may be detached from the atmosphere-model, by prescribing the atmospheric forcing.
20 In this way it has been applied to the streets of Helsinki (Fortelius and Drebs 2012). SURFEX
21 will be applied in a coupled mode as well as in a detached mode, and validated using Helsinki
22 UrBAN data, the ultimate goal being to identify and improve the representation of processes
23 particularly important to urban NWP in a high-latitude coastal environment.

24 The surface urban energy and water balance scheme SUEWS (Järvi et al. 2011) has a single-
25 layer urban surface divided into seven surface types. Above and below the ground, water flows

1 between the sub-surfaces. The model is forced using commonly-measured meteorological
2 variables (incoming solar radiation, precipitation, wind speed, air temperature, air pressure, and
3 humidity) and needs information about the surface-cover fractions of the modeled area. It
4 predicts the remaining three radiation components: turbulent fluxes of heat, water, and
5 momentum – in addition to the different components of water balance. SUEWS can be used for
6 both long-term runs of several years as well as the understanding of spatial variability.

7 Both SURFEX and SUEWS will be used to model the characteristics of the urban ABL
8 and turbulent fluxes in Helsinki. Both models will be forced using the auxiliary measurements
9 and surface-cover information.

10 Atmospheric stability parameters and ABL depth for urban scale dispersion modeling can
11 be evaluated using a meteorological preprocessing model MPP-FMI (Karppinen et al. 2000). The
12 model utilizes meteorological synoptic and sounding observations, and its output consists of
13 estimates of the relevant atmospheric turbulence parameters (the Obukhov length-scale, the
14 friction velocity, and the convective velocity scale) and ABL depth.

15 An example end-user application is the road weather model, developed at FMI, which
16 forecasts specific road weather related quantities such as road surface temperature and road
17 condition. The pedestrian slippery index model is a special version of the road weather model
18 that, instead of road weather, determines the condition existing on pavements from the
19 viewpoint of pedestrians. In contrast to the road weather model, the pedestrian model mainly
20 aims to simulate conditions in the urban environment. Dedicated and accurate predictions of
21 challenging urban conditions have been scarce because of limited information and limited
22 suitable urban environment models; there is a challenge to make accurate predictions. A
23 substantial improvement in this respect could be attained with data from Helsinki UrBAN.

1 SUPPLEMENTAL REFERENCES.

- 2 Boersma, K. F. and Coauthors, 2011: An improved tropospheric NO₂ column retrieval
3 algorithm for the Ozone Monitoring Instrument. *Atmos. Meas. Tech. Disc.*, **4**, 2329–2388.
- 4 Davies-Jones, R. P., 1979: Dual-Doppler Radar Coverage Area as a Function of Measurement
5 Accuracy and Spatial Resolution. *J. Appl. Meteor.*, **18**, 1229–1233.
- 6 Fioletov, V. E., C. A. McLinden, N. Krotkov, M. D. Moran, and K. Yang, 2011: Estimation of
7 SO₂ emissions using OMI retrievals. *Geophys. Res. Lett.*, **38**, L21811.
- 8 Fortelius, C., and A. Drebs, 2012: Intercomparison of radiative fluxes in the SURFEX TEB and
9 observations from a moving platform in the streets of Helsinki. *Hirlam NL*, **58**, 72–80.
10 http://hirlam.org/index.php?option=com_docman&task=cat_view&gid=263&Itemid=70.
- 11 Grimmond, C. S. B., and T. R. Oke, 1999: Aerodynamic Properties of Urban Areas Derived from
12 Analysis of Surface Form. *J. Appl. Meteor.*, **38**, 1262–1292.
- 13 HIRLAM-B, 2012: General description of the HARMONIE model. *HIRLAM-B*,
14 http://hirlam.org/index.php?option=com_content&view=article&id=65&Itemid=102.
- 15 Järvi, L., C. S. B. Grimmond, and A. Christen, 2011: The Surface Urban Energy and Water
16 Balance Scheme (SUEWS): Evaluation in Los Angeles and Vancouver. *J. Hydrol.*, **411**, 219–
17 237.
- 18 Kar, J., J. Fishman, J. K. Creilson, A. Richter, J. Ziemke, and S. Chandra, 2010: Are there urban
19 signatures in the tropospheric ozone column products derived from satellite measurements?
20 *Atmos. Chem. Phys.*, **10**, 5213–5222.
- 21 Karppinen, A., S. Joffre, and J. Kukkonen, 2000: The refinement of a meteorological
22 preprocessor for the urban environment. *Int. J. Environ. Poll.*, **14**, 565–572.
- 23 Kauhaniemi, M. and Coauthors, 2008: Evaluation of a modelling system for predicting the
24 concentrations of PM_{2.5} in an urban area. *Atmos. Environ.*, **42**, 4517–4529.
- 25 Koskinen, J. T. and Coauthors, 2011: The Helsinki Testbed: A Mesoscale Measurement,
26 Research, and Service Platform. *Bull. Amer. Meteor. Soc.*, **92**, 325–342.
- 27 Levelt, P. F., E. Hilsenrath, G. W. Leppelmeier, G. H. J. van den Oord, P. K. Bhartia, J.
28 Tamminen, J. F. de Haan, and J. P. Veefkind, 2006: Science objectives of the ozone
29 monitoring instrument. *IEEE Trans. Geosci. Rem. Sens.*, **44**, 1199–1208.
- 30 Lilleberg, I., and T. Hellman, 2011: The development of traffic in Helsinki in 2010 (in Finnish).
31 *Helsinki City Planning Department*, **2**, 1–70.
- 32 MacDonald, R. W., R. F. Griffiths, and D. J. Hall, 1998: An improved method for the estimation
33 of surface roughness of obstacle arrays. *Atmos. Environ.*, **32**, 1587–1864.

- 1 Masson, V., 2000: A physically-based scheme for the urban energy budget in atmospheric
2 models. *Bound.-Layer Meteor.*, **94**, 357–397.
- 3 Masson, V., and Y. Seity, 2009: Including Atmospheric Layers in Vegetation and Urban Offline
4 Surface Schemes. *J. Appl. Meteor. Climatol.*, **48**, 1377–1397.
- 5 Masson, V., J.-L. Champeaux, F. Chauvin, C. Meriguet, and R. Lacaze, 2003: A Global Database
6 of Land Surface Parameters at 1-km Resolution in Meteorological and Climate Models. *J.*
7 *Clim.*, **16**, 1261–1282.
- 8 Le Moigne, P., 2009: SURFEX scientific documentation. *SURFEX*,
9 http://www.cnrm.meteo.fr/surfex/IMG/pdf/surfex_scientific_documentation.pdf
- 10 Natunen, A., A. Arola, T. Mielonen, J. Huttunen, M. Komppula, and K. E. J. Lehtinen, 2010: A
11 multi-year comparison of PM(2.5) and AOD for the Helsinki region. *Bor. Environ. Res.*, **15**,
12 544–552.
- 13 Nordbo, A., L. Järvi, S. Haapanala, J. Moilanen, and T. Vesala, 2012: Intra-city variation in urban
14 morphology and turbulence structure in Helsinki, Finland. *Bound.-Layer Meteor.*,
15 doi:10.1007/s10546-012-9759-9.
- 16 Rantamäki, M., M. Apohjola, P. Tisler, P. Bremer, J. Kukkonen, and A. Karppinen, 2005:
17 Evaluation of two versions of the HIRLAM numerical weather prediction model during an
18 air pollution episode in southern Finland. *Atmos. Environ.* **39**, 2775–2786.
- 19 De Ruyter de Wildt, M., H. Eskes, and K. F. Boersma, 2012: The global economic cycle and
20 satellite-derived NO₂ trends over shipping lanes. *Geophys. Res. Lett.*, **39**, L01802.
- 21 Saltikoff, E., and L. Neuvonen, 2011: First experiences of the operational use of a dual-
22 polarisation weather radar in Finland. *Meteor. Zeits.*, **20**, 11.
- 23 Seity, Y., P. Brousseau, S. Malardel, G. Hello, P. Bénard, F. Bouttier, C. Lac, and V. Masson,
24 2011: The AROME-France Convective-Scale Operational Model. *Mon. Wea. Rev.*, **139**, 976–
25 991.
- 26 Suomi, I., T. Vihma, S.-E. Gryning, and C. Fortelius, 2012: Wind-gust parametrizations at heights
27 relevant for wind energy: A study based on mast observations. *Q. J. Roy. Meteor. Soc.*,
28 DOI:10.1002/qj.2039.
- 29 Tomlinson, C. J., L. Chapman, J. E. Thornes, and C. J. Baker, 2012: Derivation of Birmingham's
30 summer surface urban heat island from MODIS satellite images. *Int. J. Climatol.*, **32**, 214–
31 224.
- 32 Weng, Q., 2009: Thermal infrared remote sensing for urban climate and environmental studies:
33 Methods, applications, and trends. *ISPRS J. Photogram. Rem. Sens.*, **64**, 335–344.